International Journal of Non-Linear Mechanics 70 (2015) 2–19

Contents lists available at ScienceDirect

International Journal of Non-Linear Mechanics

journal homepage: www.elsevier.com/locate/nlm

Nonlinear dynamics and chaos in shape memory alloy systems

Marcelo A. Savi

Universidade Federal do Rio de Janeiro, COPPE – Department of Mechanical Engineering, 21.941.972 Rio de Janeiro, RJ, Brazil

ARTICLE INFO

Article history:
Received 3 December 2013
Received in revised form
8 May 2014
Accepted 6 June 2014
Available online 21 June 2014

Keywords:
Smart material systems
Shape memory alloys
Nonlinear dynamics
Chaos
Bifurcations
Non-smooth systems

ABSTRACT

Smart material systems and structures have remarkable properties responsible for their application in different fields of human knowledge. Shape memory alloys, piezoelectric ceramics, magnetorheological fluids, and magnetostritive materials constitute the most important materials that belong to the smart materials category. Shape memory alloys (SMAs) are metallic alloys usually employed when large forces and displacements are required. Applications in aerospace structures, rotordynamics and several bioengineering devices are investigated nowadays. In terms of applied dynamics, SMAs are being used in order to exploit adaptive dissipation associated with hysteresis loop and the mechanical property changes due to phase transformations. This paper presents a general overview of nonlinear dynamics and chaos of smart material systems built with SMAs. Oscillators, vibration absorbers, impact systems and structural systems are of concern. Results show several possibilities where SMAs can be employed for dynamical applications.

1. Introduction

Nature should be the essential inspiration for researchers and engineers that try to develop systems and structures. The main inspirational point is certainly the adaptive behavior that provides the self-regulation ability. Through the history, human technology is always related to different materials and it is possible to recognize ages defined by some material invention: stone and metal, for instance. Recently, smart materials should be identified as the stimulus of a new age. Basically, smart materials have a coupling between mechanical and non-mechanical fields that confers the material a special kind of behavior. In this regard, it is possible to imagine numerous applications due to the coupling of fields that usually are not connected. The smart material age tries to exploit the idea to construct systems and structures with adaptive behavior that have the ability to change properties due to environmental changes and repairing themselves when necessary.

Among many possibilities, smart materials can be classified according to the different field couplings. Nowadays, the most used materials are the shape memory alloys, the piezoelectric materials, the magnetostrictive materials and the electro- and magneto-rheological fluids. These materials have the ability of changing their shape, stiffness, among other properties, through the imposition of temperature or stress, electrical or electromagnetic fields. Smart materials are usually employed as sensors and actuators in smart structures. The choice of proper material for each application depends on many factors and two design drivers need to be highlighted [32]: the actuation energy density; and the actuation frequency.

Shape memory alloys (SMAs) present a mechanical-temperature coupling in such a way that they have the ability to recover a shape previously defined, when subjected to an appropriate thermomechanical loading process. SMA application is usually associated with high force–displacement and low frequency. The remarkable properties of SMAs are related to phase transformations responsible for different thermomechanical behaviors of these alloys. Basically, two different phases are possible in SMAs: austenite and martensite. Austenitic phase is stable at high temperatures and stress-free state presenting a single variant. On the other hand, martensitic phase is stable at low temperature in a stress-free state, being related to numerous variants. Phase transformation may be induced either by stress or by temperature. SMA thermomechanical behavior is very complex being represented by different phenomena. Pseudoelasticity, shape memory effect, two-way shape memory effect, transformation induced plasticity are some examples of important aspects of the thermomechanical behavior of SMAs.

The macroscopic behavior of SMAs can be expressed by stress–strain curves, Fig. 1. Pseudoelasticity happens at high temperatures, where the austenitic phase is stable for a stress-free state. Fig. 1a shows a typical stress–strain curve of the pseudoelastic behavior. A mechanical loading causes an elastic response until a critical stress value is reached, point A, when the martensitic transformation (austenite → detwinned martensite) arises, finishing at point B. For higher stress values, SMA presents a linear elastic response. During unloading process, the sample presents an elastic recovery ($B \rightarrow C$). From point C to D one can note the reverse martensitic transformation (detwinned martensite → austenite).

E-mail address: savi@mecanica.ufrj.br

http://dx.doi.org/10.1016/j.ijnonlinmec.2014.06.001
0020-7462/

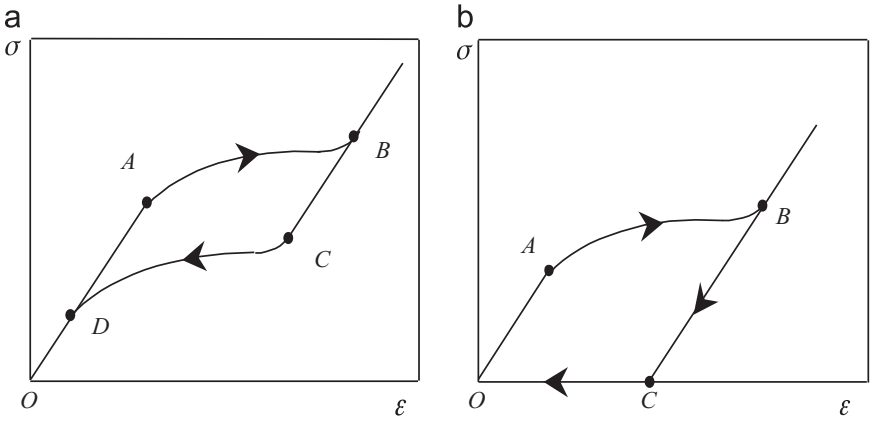

Fig. 1. SMA macroscopic behavior represented by stress–strain curves: (a) pseudoelasticity and (b) shape memory effect.

Afterward, the sample presents an elastic discharge. When the loading–unloading process is finished, SMA has no residual strain, however, there is an energy dissipation represented by the hysteresis loop.

The position of this hysteresis loop is temperature dependent and, since the temperature goes down, the hysteresis loop moves down as well. For low temperature behavior, the hysteresis position can be such that there is a residual strain after the loading–unloading process. Fig. 1b shows the stress–strain curve related to the shape memory effect. Basically, the martensitic phase is the only stable phase under this condition. When the sample is subjected to a mechanical loading, the stress reaches a critical value, point *A*, beginning the reorientation from the twinned into the detwinned martensite, ending at point *B*. During the unloading process, the SMA sample presents a linear elastic response, resulting in a residual strain (Point *C*). This residual strain can be recovered through a sample's heating, which induces the martensite–austenite phase transformation.

The description of SMA thermomechanical behavior is the objective of several research efforts. The constitutive modeling is related to phenomenological features to take into account the changes in the microstructure due to phase transformation [46,45]. Paiva and Savi [45] and Lagoudas [32] presented a general overview of the SMA modeling, with the emphasis on the phenomenological constitutive models.

The remarkable properties of SMAs are attracting technological interest in several fields of sciences and engineering. Machado and Savi [35] presented an overview of the most relevant SMA applications within biomedical field. The success of SMA biomedical applications is due to the non-invasive characteristic of SMA devices and also due to their excellent biocompatibility. SMAs are usually employed in surgical instruments, cardio-vascular, orthopedic and orthodontic devices, among other applications. Self-expansive structures constitute one of the main applications of SMAs, as the Simon filters and stents.

Besides biomedical applications, SMAs have been investigated to applications in engineering fields. Paiva and Savi [45] and Lagoudas [32] discussed some of the most important engineering applications. Self-expanded structures are employed to promote deployments and to establish connections. Another interesting application is related to multi-actuated flexible structures that can be applied in hydrofoils or wings. Robotic applications are also exploiting SMA characteristics, trying to mimic the continuous movement of muscles that is important for the construction of members as hands, arms and legs. Besides, automotive applications are also considering the use of SMAs for different purposes [17].

Dynamical systems with SMA elements constitute another important field of potential application being associated with both the adaptive dissipation of energy related to their hysteretic behavior and large changes in their mechanical properties caused by phase transformations. These aspects can be exploited both in the adaptive–passive and the active control, and a limiting factor is the slow rate of response. SMA is also being used in impact systems where it is expected that the high dissipation capacity due to hysteresis loop results in less complex behaviors. This can dramatically changes the system response when compared to those obtained with an equivalent linear elastic impact [48,62,61].

The dynamical response of SMA systems has complex dynamical responses including chaos and hyperchaos. The investigation of SMA oscillators is treated in different studies showing the general complexity of the nonlinear dynamics of SMA systems [49,50,36,37,38,30,31,10,11,12,9,54]. Aguiar et al. [3] presented an experimental investigation of SMA oscillators showing some of these complex behaviors. Doaré et al. [23] discussed torsional behavior of SMA systems. Besides, it is important to mention some efforts related to the characterization of chaos using either Lyapunov exponents [38] or 0–1 test [34].

SMA structures have been investigated by different approaches. The finite element method is an important tool to this aim. Concerning dynamical applications, Gholampour et al. [25] discussed some aspects of smart structures with SMA members. Collet et al. [16] analyzed the dynamical response of SMA beams, as well as Auricchio and Sacco [5]. De Paula et al. [19] treated an SMA grid employed for aerospace applications. Savi and Nogueira [57] and Savi et al. [51] discussed two-bar trusses with SMA elements.

Hybrid composites with SMA actuators are another application for shape and buckling control and also to change natural frequencies. Hajianmaleki and Qatu [26] presented a general review about vibration of composite beams, including the ones with SMA members. Nonlinear dynamic response of sandwich beams with SMAs is treated in Khalili et al. [29] using the finite element method. Shariyat et al. [58] presented the nonlinear dynamics analysis of rectangular composite plates with SMA wires.

The use of SMAs for control purposes is vast. The tuned vibration absorber (TVA) is a passive vibration control device for achieving reduction in the vibration of a primary system subject to external excitation. The TVA consists of a secondary oscillatory system that once attached to the primary system is capable of absorbing vibration energy from the primary system. An alternative for systems where the forcing frequency varies or has a kind of uncertainty is the concept of an adaptive tuned vibration absorber. This device is similar to a TVA but with adaptive elements that can be used to change the tuned condition [1,63,27,14]. Savi et al. [56] discussed the use of SMAs in tuned vibration absorber and Williams et al. [65] investigated a

prototype of this device. Adaptive–passive vibration control has been applied on bridges [22,64] and other civil structures subjected to earthquakes [15,47]. Amarante dos Santos et al. [4] treated semi-active vibration control using a device with SMA wires. Bessa et al. [13] and De Paula et al. [21] presented different approaches of nonlinear control to the SMA two-bar truss.

This paper presents a general overview of applied dynamics involving shape memory alloy systems. SMA oscillators, vibration absorbers, impact and structural systems are of concern. A collection of results is chosen in order to show the general aspects of the dynamical behavior of SMA systems. Some experimental results are presented confirming the main conclusions.

2. Mathematical modeling and constitutive models

The modeling and simulation of the thermomechanical behavior of SMAs is the objective of numerous research efforts being a complex subject. The constitutive modeling is related to phenomenological features to take into account the changes in the microstructure due to phase transformation [46,45]. Paiva and Savi [45] and Lagoudas [32] presented a general overview of the SMA modeling, with the emphasis on the phenomenological constitutive models. The SMA modeling becomes even more complex when three-dimensional media is of concern. Although many constitutive models are developed for a three-dimensional description, their verification is difficult due to the lack of experimental data. Oliveira et al. [41] proposed a constitutive model for three-dimensional media, presenting a literature review about the subject.

Among many alternatives of SMA constitutive models, there is a class of models in literature known as models with assumed phase transformation kinetics that, probably are the most popular in the literature, playing an important role within the SMA's modeling. Another possibility is a model with internal constraints, originally based on Fremond [24]. This model was the objective of several improvements reported in the following references: Paiva et al. [44], Savi and Paiva [53], Baêta-Neves et al. [7], Savi et al. [52], Aguiar et al. [2] and Monteiro et al. [39].

Constitutive equations should be developed within a proper formalism. A remarkable procedure is the framework of continuum mechanics employing the generalized standard material approach [33]. On this basis, the thermomechanical behavior of a continuum may be modeled from the Helmholtz free energy density, Ψ, and the pseudo-potential of dissipation, Φ in order to satisfy the second law of thermodynamics. A brief discussion about this procedure is now presented. Consider the local form of the Clausius–Duhem inequality:

$$\sigma\dot{\varepsilon}-\rho(\dot{\Psi}+s\dot{T})-qg\geq 0 \tag{1}$$

where the dot means time derivative, ρ is the density, s is the specific entropy, T is the temperature, σ is the stress, ε is the total strain, q is the heat flux and $g=\frac{1}{T}\frac{\partial T}{\partial x}$, where x represents the spatial coordinate.

As a first hypothesis concerning the constitutive modeling, it is assumed that the Helmholtz free energy density is a function of a finite set of variables:

$$\Psi=\Psi(\varepsilon,T,\beta) \tag{2}$$

where β represents a set of internal variables. Since $\dot{\Psi}=\frac{\partial\Psi}{\partial\varepsilon_{ij}}\dot{\varepsilon}+\frac{\partial\Psi}{\partial T}\dot{T}+\frac{\partial\Psi}{\partial\beta}\dot{\beta}$, the Clausius–Duhen inequality is rewritten as follows:

$$\left(\sigma-\rho\frac{\partial\Psi}{\partial\varepsilon}\right)\dot{\varepsilon}-\rho\left(s+\frac{\partial\Psi}{\partial T}\right)\dot{T}-\rho\frac{\partial\Psi}{\partial\beta}\dot{\beta}-qg\geq 0 \tag{3}$$

This form motivates the following definitions of the thermodynamical forces, related to reversible part of the process.

$$\sigma^R=\rho\frac{\partial\Psi}{\partial\varepsilon};\quad B=-\rho\frac{\partial\Psi}{\partial\beta};\quad s^R=-\frac{\partial\Psi}{\partial T} \tag{4}$$

In order to describe irreversible processes, complementary laws are defined from a pseudo-potential of dissipation that is a function of internal variables:

$$\Phi=\Phi(\dot{\varepsilon},\dot{\beta},\dot{T},q) \tag{5}$$

The thermodynamical formalism establishes thermodynamics fluxes as follows [33,24]:

$$\sigma^I=\frac{\partial\Phi}{\partial\dot{\varepsilon}};\quad B=\frac{\partial\Phi}{\partial\dot{\beta}};\quad s^I=\frac{\partial\Phi}{\partial\dot{T}};\quad g=\frac{\partial\Phi}{\partial q} \tag{6}$$

Alternatively, these thermodynamic fluxes may be obtained from the dual of the potential of dissipation $\Phi^*(\sigma^I,B,s^I,g)$ allowing the definitions:

$$\dot{\varepsilon}^I=\frac{\partial\Phi^*}{\partial\sigma^I};\quad \dot{\beta}=\frac{\partial\Phi^*}{\partial B};\quad \dot{T}=\frac{\partial\Phi^*}{\partial s^I};\quad q=\frac{\partial\Phi^*}{\partial g} \tag{7}$$

where ε^I is the irreversible strain.

On this basis, a complete set of constitutive equations is defined:

$$\sigma=\rho\frac{\partial\Psi}{\partial\varepsilon}+\frac{\partial\Phi}{\partial\dot{\varepsilon}} \tag{8}$$

$$B=-\rho\frac{\partial\Psi}{\partial\beta}=\frac{\partial\Phi}{\partial\dot{\beta}} \tag{9}$$

$$s=-\frac{\partial\Psi}{\partial T}-\frac{\partial\Phi}{\partial T} \tag{10}$$

$$g=\frac{\partial\Phi}{\partial q} \tag{11}$$

In general, if the pseudo-potential Φ is a positive convex function that vanishes at the origin, the Clausius–Duhen inequality is automatically satisfied.

In order to consider thermomechanical couplings, it is necessary to establish the energy conservation equation given by the first law of thermodynamics:

$$\rho\dot{\Psi}=\sigma\dot{\varepsilon}-\frac{\partial q}{\partial x}-\rho T\dot{s}-\rho\dot{T}s \tag{12}$$

By considering a single point description, spatial variations are neglected. Besides, a convection boundary condition is assumed. Therefore, the first law of thermodynamics has the following form:

$$\rho c_p\dot{T}=-h(T-T_\infty)+\sigma\dot{\varepsilon}^I+B\dot{\beta}+T\left[\frac{\partial\sigma}{\partial T}(\dot{\varepsilon}-\dot{\varepsilon}^I)-\frac{\partial B}{\partial T}\dot{\beta}\right] \tag{13}$$

where c_p is the specific heat at constant pressure, h is the convection coefficient, T_∞ is the environmental temperature. The first term on the equation right side is the convection term whereas the others are associated with the thermomechanical couplings.

Specifically, SMA description using the model with internal constraints assumes as variables the total strain, ε, the temperature, T, and four internal variables that represent volume fraction of each macroscopic phase: β^+ and β^-, related to detwinned martensites, respectively associated with tension and compression; β^A that represents the austenitic volume fraction; and β^M that represents the volume fraction of twinned martensite. Since there is a constraint based on phase coexistence, $\beta^++\beta^-+\beta^A+\beta^M=1$, it is possible to use only three volume fractions and the thermomechanical behavior of the SMA is described by the following set of equations:

$$\sigma=E\varepsilon+[E\alpha_h+\alpha](\beta^--\beta^+)-\Omega(T-T_0) \tag{14}$$

$$\dot{\beta}^{+} = (1/\eta^{+})\{\alpha\varepsilon + \Lambda^{+}(T) + (2\alpha\alpha_h + E\alpha_h^2)(\beta^{-} - \beta^{+}) + \alpha_h[E\varepsilon - \Omega(T - T_0)] - \partial_{\beta^{+}} J_\pi\} + \partial_{\dot{\beta}^{+}} J_\chi \tag{15}$$

$$\dot{\beta}^{-} = (1/\eta^{-})\{-\alpha\varepsilon + \Lambda^{-}(T) - (2\alpha\alpha_h + E\alpha_h^2)(\beta^{-} - \beta^{+}) - \alpha_h[E\varepsilon - \Omega(T - T_0)] - \partial_{\beta^{-}} J_\pi\} + \partial_{\dot{\beta}^{-}} J_\chi \tag{16}$$

$$\dot{\beta}^{A} = (1/\eta^{A})\Big\{-(1/2)(E_A - E_M)[\varepsilon + \alpha_h(\beta^{-} - \beta^{+})]^2 + \Lambda^{A}(T) + (\Omega_A - \Omega_M)(T - T_0)[\varepsilon + \alpha_h(\beta^{-} - \beta^{+})] - \partial_{\beta^{A}} J_\pi\Big\} + \partial_{\dot{\beta}^{A}} J_\chi \tag{17}$$

where $E = E^M + \beta^A (E^A - E^M)$ is the elastic modulus while $\Omega = \Omega^M + \beta^A(\Omega^A - \Omega^M)$ is related to thermal expansion coefficient. Note that subscript A refers to austenitic phase, while M refers to martensite. Parameters $\Lambda^+ = \Lambda^- = \Lambda = \Lambda(T)$ and $\Lambda^A = \Lambda^A(T)$ are associated with phase transformation stress levels. Parameter α_h defines the horizontal width of the stress–strain hysteresis loop, while α controls the height of the same hysteresis loop. The terms $\partial_n J_\pi$ ($n = \beta^+, \beta^-, \beta^A$) are sub-differentials of the indicator function J_π with respect to n. This indicator function is related to a convex set π, which provides the internal constraints related to the phase coexistence. With respect to evolution equations of volume fractions, $\eta^+ = \eta^- = \eta$ and η^A represent the internal dissipation related to phase transformations. Moreover $\partial_n J_\chi$ ($n = \beta^+, \beta^-, \beta^A$) are sub-differentials of the indicator function J_χ with respect to n. This indicator function is associated with the convex set χ, which establishes conditions for the correct description of internal sub-loops due to incomplete phase transformations. These sub-differentials may be replaced by Lagrange multipliers associated with the mentioned constraints.

Concerning parameter definitions, temperature dependent relations are adopted for Λ and Λ^A as follows:

$$\Lambda = \begin{cases} -L_0 + \frac{L}{T_M}(T - T_M), & \text{if} \quad T > T_M \\ -L_0, & \text{if} \quad T \le T_M \end{cases}; \quad \Lambda^A = \begin{cases} -L_0^A + \frac{L^A}{T_M}(T - T_M), & \text{if} \quad T > T_M \\ -L_0^A, & \text{if} \quad T \le T_M \end{cases} \tag{18}$$

where T_M is the temperature below where the martensitic phase becomes stable. Usually, experimental tests provide information of M_s and M_f, temperatures of the start and finish of the martensitic formation. This model uses only one temperature that could be an average value or alternatively, the M_s value. Moreover, L_0, L, L_0^A and L^A are parameters related to critical stress for phase transformation.

In order to describe the characteristics of phase transformation kinetics, different values of η and η^A can be considered during loading, η_L and η_L^A, and unloading processes, η_U and η_U^A.

As it is well-known, SMA devices demonstrate time-dependent characteristics which means that their thermomechanical response depends on the loading rate, see e.g., Shaw and Kyriakides [59] and Yoon [66]. The adequate modeling of this time-dependency can be performed by considering the thermomechanical coupling terms in the energy equation. Monteiro Jr. et al. [39] discussed this approach in SMAs. Monteiro et al. [40] presented some experimental results related to the rate dependent behavior of SMA actuators. The considered constitutive model has viscous characteristics that allow the description of the thermomechanical coupling avoiding the integration of the energy equation, presenting useful results [2]. This rate dependent aspect can be controlled by the proper choice of model parameters. Auricchio et al. [6] explored this idea showing the difference between a viscous model and a rate-independent model with thermomechanical coupling. Both models have the ability to describe pseudoelastic and shape memory behavior in SMA wires. For more details about the constitutive model see Paiva et al. [44].

2.1. Numerical procedure

In order to deal with nonlinearities of the constitutive model formulation, a numerical procedure based on operator split technique is developed [43]. The basic idea is to split the state space in order to treat the set of governing equations in a decoupled way. Therefore, the constitutive equations are solved by assuming a predictor–corrector approach. The predictor step is defined by assuming a trial state where phase transformation does not take place. If the constraints are satisfied, this trial state is the actual one. Otherwise, a projection algorithm is employed calculating the sub-differentials of the constitutive equations. This sequence is repeated until a prescribed tolerance is reached [52].

In terms of more general systems, the operator split technique can be employed together with other numerical procedures, promoting a new split of the state space. In dynamical systems, for instance, it is defined a subspace with the dynamical variables (position and velocity for a single degree of freedom oscillator), and constitutive variables define another subspace. They can be solved in a separate form and an iterative procedure assures the system convergence [54]. Any classical procedure can be employed to perform the integration of a specific subspace. The fourth order Runge-Kutta method is a good alternative for the dynamical subspace. The projection algorithm is the proper alternative for the constitutive model subspace. Fig. 2 presents a schematic picture of the operator split approach. The dynamical box represents the dynamical subspace that can be solved using the Runge-Kutta method, for instance, assuming that other state variables remain constant. Afterward, this result is used as an input for the constitutive model subspace, represented by the box constitutive model. This procedure considers the projection algorithm employed for quasi-static situations. Note that the constitutive model box is related to a new operator split.

In general, this constitutive model can capture the general thermomechanical behavior of SMAs, presenting a close agreement with experimental data. Fig. 3 shows a collection of results

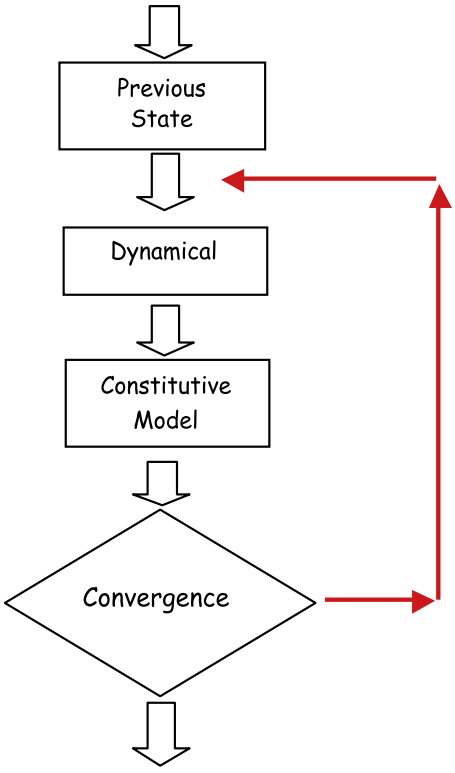

Fig. 2. Numerical procedure.

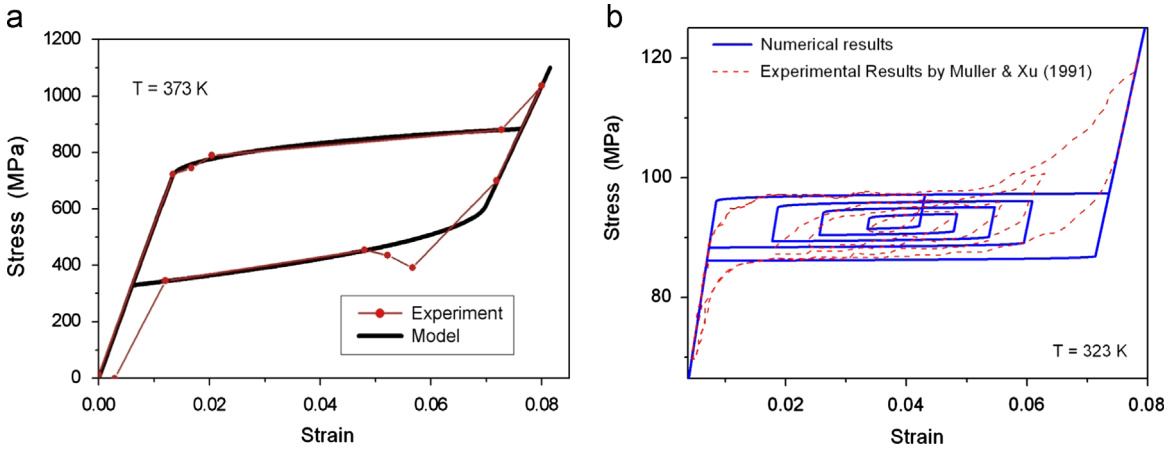

Fig. 3. SMA description using a constitutive model with internal constraints (a) Pseudoelasticity and (b) internal subloops [53].

showing the comparison between numerical simulations and experimental data reported in literature [44,53].

3. SMA oscillator

The dynamical analysis of SMA systems starts with a single-degree of freedom oscillator (Fig. 4), where the restitution force, F_R, is provided by an SMA element. This is an archetypal model of several engineering systems. The non-dimensional equations of motion is given by Savi et al. [54], where the volume fractions are calculated from the constitutive equations presented in the previous section.

$$U''+\xi U'+\mu_E U+(\overline{\alpha}+\mu_E\overline{\alpha}_h)(\beta^- -\beta^+)-\mu_\Omega\overline{\Omega}(\theta-\theta_0)=\delta\ \sin(\varpi\tau) \quad (19)$$

where μ_E, μ_Ω, ξ, δ, ϖ are system parameters; $\theta=T/T_M$ represents a non-dimensional temperature. The thermomechanical description of the restitution force of the SMA element is modeled by the force F_R, representative of different SMA elements that can include bars and springs, for instance. A bar element can be described by $F_R=\sigma A$ where the stress is described by the constitutive equation presented in the previous section. Aguiar et al. [2] showed that the spring force–displacement curve can be modeled by assuming that both phase transformation and shear stress distributions are homogeneous through the wire cross section. Although this hypothesis is not completely realistic, its simplicity can be useful for several purposes resulting in a force–displacement relation that is equivalent to the stress–strain relation presented in the previous section. This spring model has results that are in close agreement with experimental data presented in Aguiar et al. [2].

Fig. 5 presents the SMA spring response for different temperatures, establishing a comparison between numerical and experimental results. Basically, pseudoelastic test is performed by considering an applied electric current of 0.8 A, that increases the SMA temperature, promoting a phase transformation from twinned martensite to austenite. Afterward, mechanical loading–unloading process is imposed to the spring by considering two different maximum values: 7 N and 8 N. Shape memory effect test is performed by imposing a mechanical loading that promotes the formation of detwinned martensite. This phase remains after the mechanical loading removal, causing a residual displacement. An electric current of 1.2 A is then applied and the SMA helical spring recovers part of the residual displacement developed during the loading stage. A residual load with a magnitude of approximately 1 N is still present at the end of the unloading as a consequence of the devices attached to the spring.

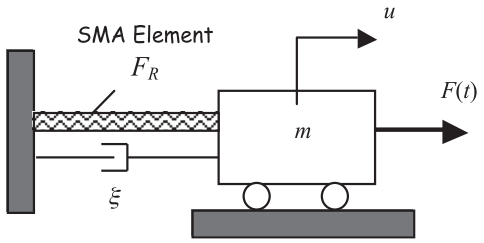

Fig. 4. Single-degree of freedom SMA oscillator.

The free vibration response of the SMA oscillator is characterized by different structures of equilibrium points depending on temperature. The oscillator free response is illustrated analyzing a system without viscous damping ($\xi=0$). Results from simulations are presented in the form of phase portraits. Fig. 6 presents the free response of a system at different temperatures: $\theta=1.28$, representing a high temperature where austenite is stable for a stress-free state; and $\theta=0.99$, a low temperature where martensite is stable for a stress-free state. Between these two temperatures, martensite and austenite may coexist and it represents a transition region between the two cited situations [50,36,37]. For high temperatures, there is only a single equilibrium point. The system response presents dissipation for high amplitudes, converging to an elastic orbit near the equilibrium point, where phase transformations do not take place anymore. This behavior is due to hysteresis loop and the absence of energy dissipation in the linear-elastic region. For low temperatures, the dissipation characteristics are similar to the high temperature behavior but there is an increase of the number of equilibrium points. By observing the phase portrait, it is noticeable three stable equilibrium points, related to different martensitic variants. This scenario suggests the existence of unstable points among the stable ones.

The existence of different equilibrium points may be exploited together with the temperature dependence in various applications. In order to illustrate this behavior, it is shown a simulation where temperature varies as indicated in Fig. 7a, by increasing system temperature between two levels. Figs. 7b and 7c show the system response, presenting time history and phase space, respectively. Notice that the system oscillates around one point at low temperature, changing its oscillation position when temperature increases. This simulation illustrates the potentiality of SMA to be used as actuators for position control.

Aguiar et al. [3] presented experimental results that confirm these numerical simulations. The experimental apparatus is a car free to move over a rail and an electrical power provides energy

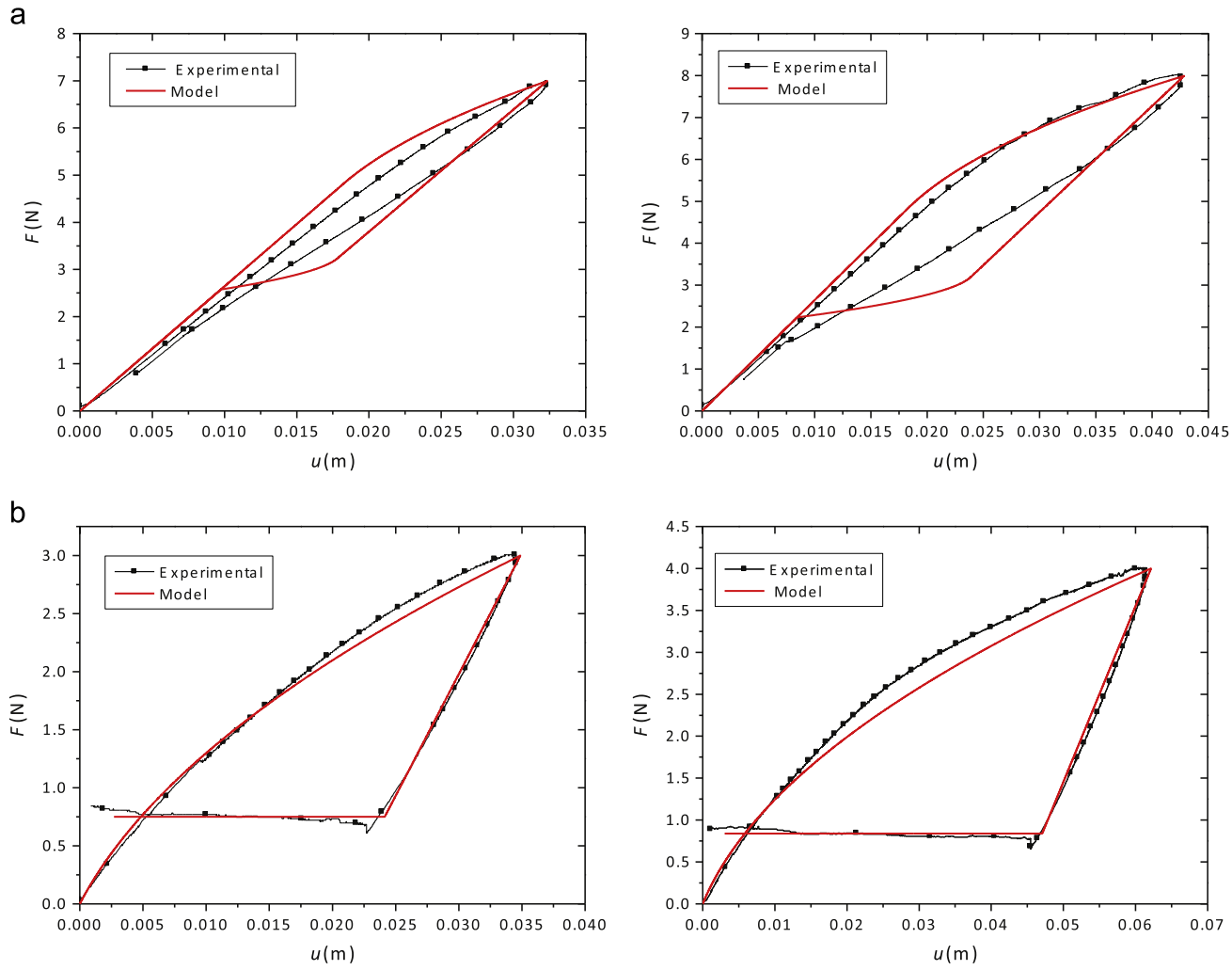

Fig. 5. SMA spring description using a constitutive model with internal constraints and experimental data [2]. (a) Pseudoelasticity and (b) shape memory effect.

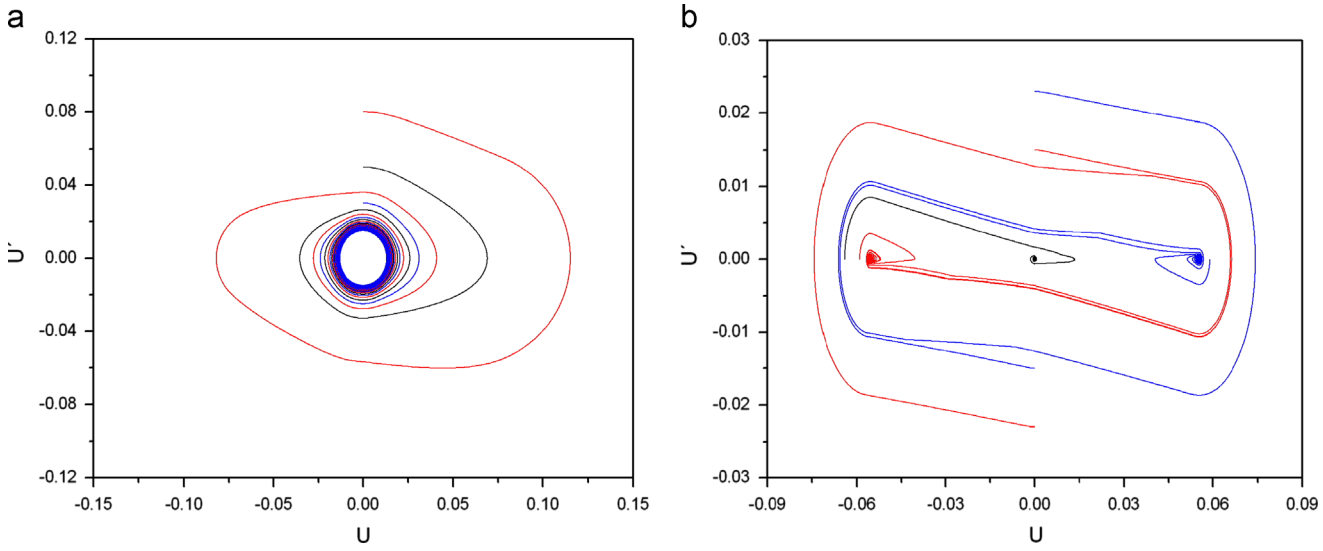

Fig. 6. SMA oscillator phase portraits at different temperatures [54]. (a) $\theta=1.28$ and (b) $\theta=0.99$.

for temperature variations. Fig. 8a shows a schematic picture of the experimental apparatus. Free vibrations of this setup are evaluated by considering perturbations to the system. Essentially, the perturbation induces a change in displacement that represents initial conditions to the car at two different temperatures (obtained by applying an electric current on the SMA helical spring). After this, the car is free to move. Fig. 8b presents the general analysis of free vibrations showing the application of different initial conditions for two different temperatures and the consequent system response. Initially, the system is at rest

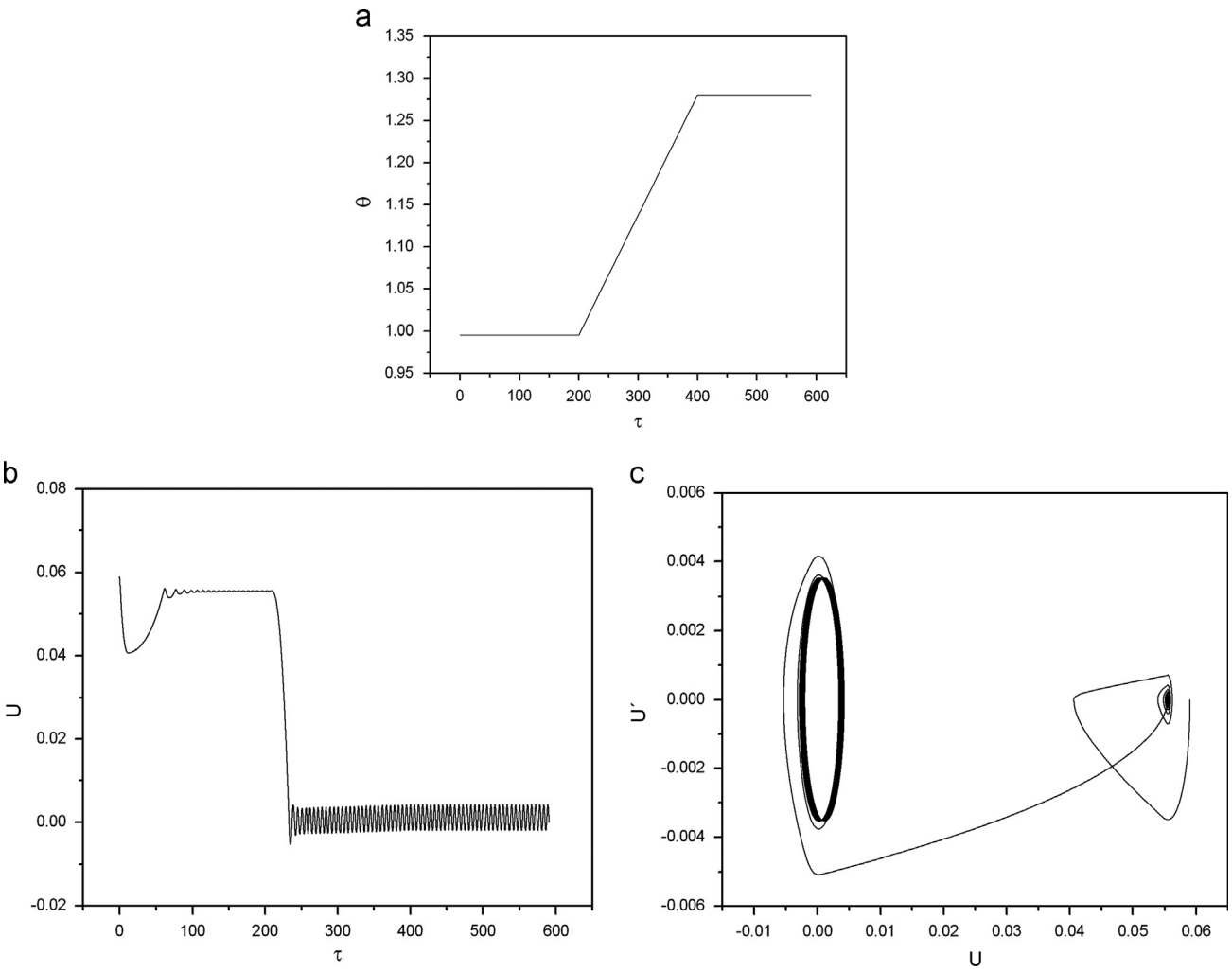

Fig. 7. SMA oscillator free vibration due to temperature variations [54]. (a) Temperature loading; (b) displacement time history; and (c) phase space.

when a perturbation of 1 mm is imposed to the car. This perturbation generates oscillations around the same equilibrium point that decreases until the system returns to the rest. It should be highlighted that the attenuation is caused by the system dissipation, mainly due to hysteretic behavior of the SMA spring. A greater perturbation is then imposed to the system (7.3 mm) and as a consequence, the system oscillates around a new position (-1 mm). Note that the system presents the same qualitative behavior, but oscillates around a different position. A temperature increase is then imposed to the system by applying an electric current of 1.8 A to the SMA spring. This temperature increase changes the equilibrium position again inducing the martensite–austenite phase transformation. Under this condition, new perturbations are imposed to the system. Initially, a 3.2 mm displacement is imposed that is followed by oscillations around this position. Afterward, a 9.5 mm perturbation is imposed and the system presents the same qualitative behavior, oscillating around the same position.

Concerning forced vibrations of SMA systems, several situations can be imagined. An important application related to SMA dynamical behavior is the idea of the smart dissipation due to hysteresis loop. A paradigmatic way to visualize this kind of behavior is obtained by considering the system response under resonant conditions. As it is well-known, a non-dissipative linear system (where SMA element is replaced by a linear element) tends to increase the response amplitude indefinitely under this condition (Fig. 9a). The shape memory alloy system, on the other hand, tends to dissipate higher energy levels as the response amplitude grows. This is due to phase transformation related to the hysteresis loop and therefore, the amplitude tends to stabilize in lower values, as shown in Fig. 9b. This behavior is interesting to be exploited as a passive vibration control.

The SMA dynamical system can present complex behavior due to its strong nonlinearities. At this point, low temperature behavior (where martensite is stable for a stress-free state) is of concern. In order to perform a global analysis, bifurcation diagrams are constructed, performing a stroboscopic sampling of the position against the slow quasi-static variation of the forcing amplitude parameter. Fig. 10 shows bifurcation diagrams obtained using two different procedures. The first considers similar initial conditions for each parameter value (Fig. 10a) while the second procedure considers stabilized values of state variables as initial conditions for the next parameter value (Fig. 10b). Bifurcation diagrams presented in Fig. 10 show different clouds of points that appear by the consideration of different employed procedures. It is important to observe that, actually, there are three coexisting steady state solutions related to this region (a symmetric cloud of points can be obtained changing initial conditions of the bifurcation diagram of Fig. 10a).

The forthcoming analysis exploits the multi-stability behavior related to coexisting attractors by changing initial conditions. Therefore, forcing parameter is considered in a region associated with $\delta = 3 \times 10^{-3}$ of the bifurcation diagram. Fig. 11 presents the system response for three different situations with the same set of

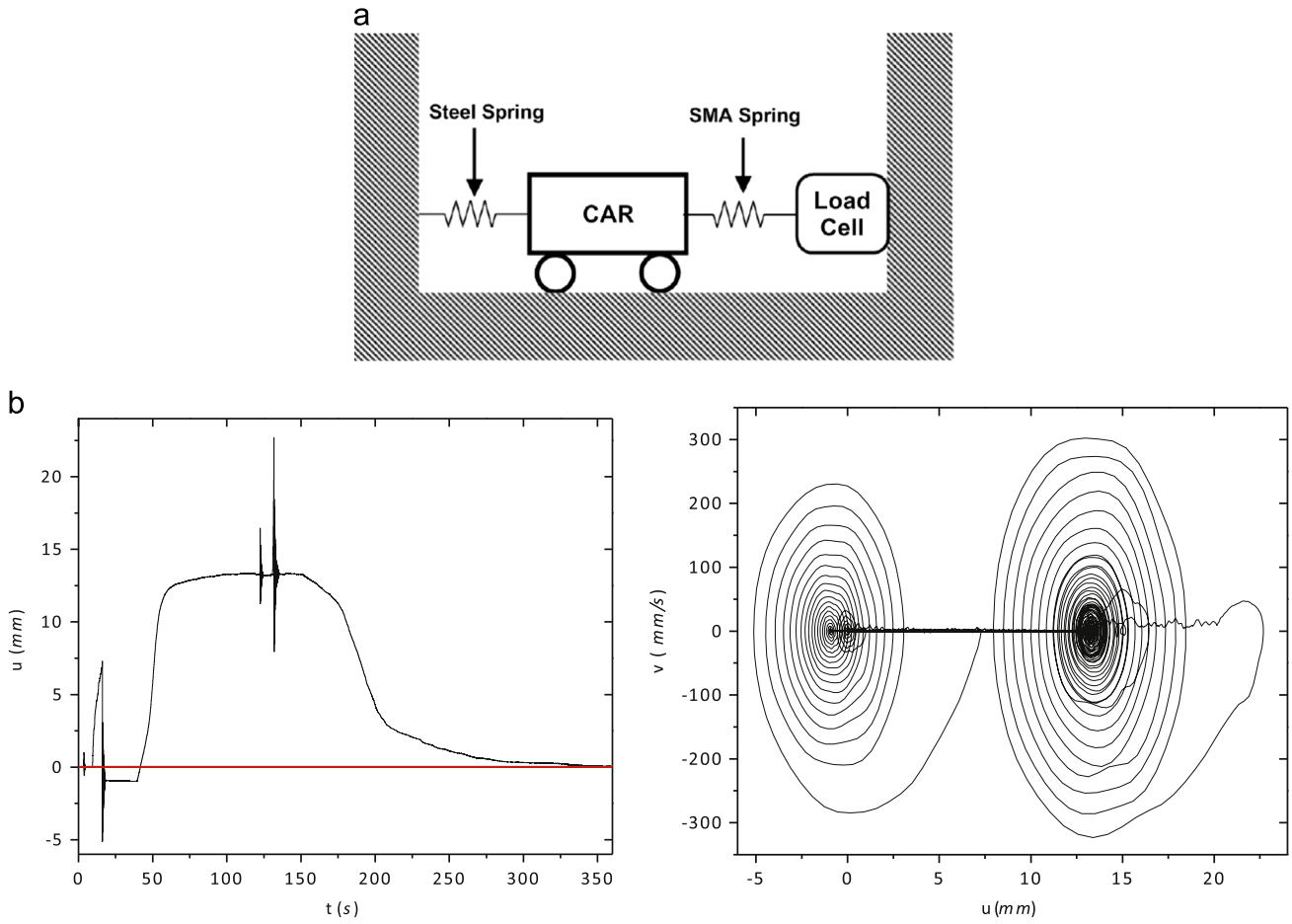

Fig. 8. Experimental SMA oscillator free vibration due to temperature variations [3]. (a) Experimental apparatus and (b) system response.

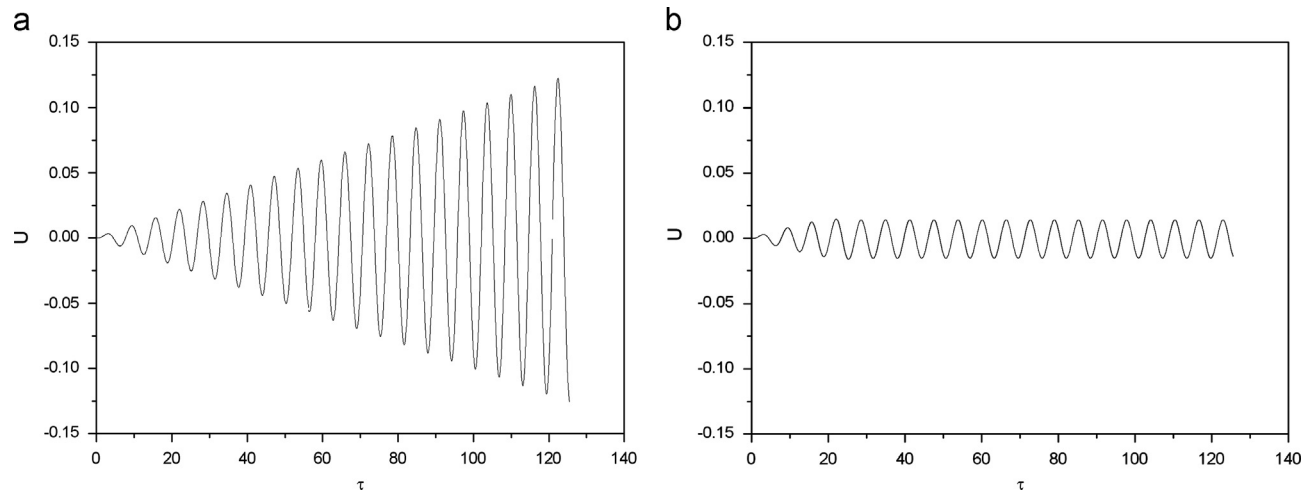

Fig. 9. SMA oscillator passive control exploiting hysteresis dissipation [54,56]. (a) Linear element and (b) SMA element.

parameters. Basically, phase space plots and Poincaré sections are presented for each response. A period-1 response may be obtained considering initial conditions near the steady state solution presented in Fig. 10b. Under this condition, the system oscillates around the null equilibrium point (Fig. 11a). By assuming initial conditions within the cloud of points presented in Fig. 10a, a chaotic-like response occurs, being related to oscillations in the positive part of the phase space (Fig. 11b). Finally, the third steady state response may be obtained assuming initial conditions within the symmetric cloud of point (not shown in Fig. 10a). Under this condition, the system presents a chaotic-like response that occurs in the negative part of the phase space (Fig. 10c).

4. SMA vibration absorber

The tuned vibration absorber (TVA) is a passive vibration control device for achieving vibration reduction of a primary system subjected to external excitation by connecting a secondary system. The adaptive tuned vibration absorber (ATVA) is an adaptive–passive

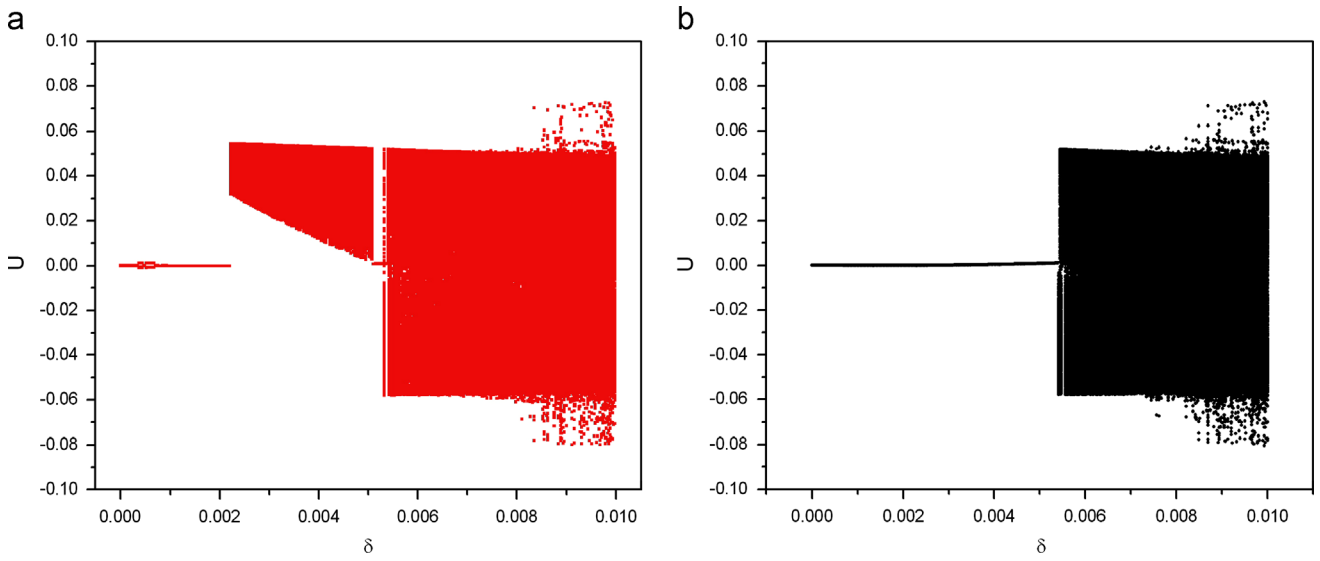

Fig. 10. SMA oscillator bifurcation diagrams for $\xi=5\times10^{-6}$ and $\varpi=1$ [54]. (a) Similar initial conditions for each parameter and (b) stabilized values of state variables as an initial condition for the next parameter value.

vibration control device similar to a TVA but with adaptive elements that can be used to change the ATVA tuned condition. The aim of ATVAs with SMA elements (SMA–ATVA) is to attenuate primary system vibration amplitudes, not only for one specific forcing frequency, as occurs with the TVA, but for a range of frequencies exploring the temperature dependent characteristic of the SMAs. This section investigates the SMA–ATVA dynamics by establishing a comparison between two different absorbers [56]: a TVA and an SMA–ATVA. Fig. 12 presents a two-degree of freedom system that represents a primary system, subsystem (m_1,c_1,k_1), that is harmonically excited by an external force $F=F_0\sin(\omega t)$. The goal is to reduce vibration amplitudes by using a secondary system that consists of a concentrated mass, m_2, attached to a viscous damper with coefficient, c_2, and to an element with restoring force F_R. This element could be an SMA element with length l and transversal section area A, defining an SMA–ATVA system or a linear elastic element defining a classical TVA.

The SMA–ATVA systems may be described by the following non-dimensional equations of motion equations together with constitutive model previously discussed to define volume fractions evolutions [56]:

$$\begin{cases} U''_1+(\xi_1+\gamma_m\xi_2)U'_1-\gamma_m\xi_2U'_2+\gamma_\omega U_1+\gamma_m[-\mu_E(U_2-U_1)-(\overline{\alpha}+\mu_E\overline{\alpha}_h)(\beta^- -\beta^+)+ \\ +\mu_\Omega\overline{\Omega}(\theta-\theta_0)]=\delta sin(\varpi\tau) \\ U''_2-\xi_2U'_1+\xi_2U'_2+\mu_E(U_2-U_1)+(\overline{\alpha}+\mu_E\overline{\alpha}_h)\beta^- -\beta^+)-\mu_\Omega\overline{\Omega}(\theta-\theta_0)=0 \end{cases} \tag{20}$$

The TVA has a linear restitution force that results in the following dynamical system expressed as dimensionless equations as follows.

$$\begin{cases} U''_1+\left(\xi_1+\frac{m_2}{m_1}\xi_2\right)U'_1-\frac{m_2}{m_1}\xi_2U'_2+\left(\frac{\omega_{L1}^2}{\omega_{02}^2}+\frac{m_2}{m_1}\frac{\omega_{L2}^2}{\omega_{02}^2}\right)U_1-\frac{m_2}{m_1}\frac{\omega_{L2}^2}{\omega_{02}^2}U_2=\delta sin(\varpi\tau) \\ U''_2-\xi_2U'_1+\xi_2U'_2-\frac{\omega_{L2}^2}{\omega_{02}^2}U_1+\frac{\omega_{L2}^2}{\omega_{02}^2}U_2=0 \end{cases} \tag{21}$$

where $\omega_{L1}^2=k_1/m_1$, $\omega_{01}^2=k/m_1$ and $\omega_{L2}^2=k_L/m_2$, respectively representing the isolated natural frequencies of primary and secondary systems.

Fig. 13 presents a comparison between the TVA and the SMA–TVA responses. Fig. 13a presents the response of the TVA primary system showing the maximum amplitudes as a function of the forcing frequency. These results are compared with the single-degree of freedom oscillator (1DoF) response. It can be observed that the absorber attenuates the critical resonant situation for the 1DoF oscillator. Nevertheless, the new degree of freedom related to the secondary system introduces two resonant frequencies. Fig. 13b shows the SMA–ATVA response by considering two different temperatures. Note that it is possible to change the range of frequencies where the primary system amplitude reduction is achieved by changing the temperature. This kind of behavior increases the frequency range where the ATVA can be efficiently used, which is an essential advantage when compared to the elastic TVA.

Aguiar et al. [3] presented experimental results that confirm these numerical simulations. The experimental apparatus is a two-degrees of freedom system (2DoF) composed by cars free to move over a rail and an electrical power provides energy for temperature variations. Besides, a shaker provides a sinusoidal excitation of 0.25 g acceleration amplitude. The excitation frequency signal changes linearly during the test from 6 to 18 Hz with 0.02 Hz/s. Results for the 2Dof are compared with results for elastic one-degree of freedom system in order to evaluate the performance of the SMA absorber. Fig. 14 presents acceleration curves for the 1DoF system and for the 2DoF system with two different electric currents: 0.8 and 2.0 A. It should be highlighted that the temperature change alters the system response of the SMA system, changing the tuned frequency of the SMA absorber. This confers an adaptive characteristic for the SMA absorber.

Although temperature-induced phase transformations can provide flexibility to the SMA–ATVA behavior when compared to the classical TVA, the system response should be better explored by assuming large amplitudes of the SMA element that causes stress-induced phase transformations related to hysteretic behavior. The analysis of dynamical jumps is essential for a proper design of the SMA–ATVA. This analysis is now of concern by considering the influence of forcing frequency variation on system response. Bernardini and Rega [9] and Oliveira et al. [42] presented discussions related to these jumps in SMA one-degree of freedom systems. Fig. 15 presents results associated with the SMA–ATVA system subjected to sine-sweep tests, plotting together the 1DoF and the TVA responses allowing a proper comparison among all results. Note that dynamical jumps are close to the first natural frequency of the TVA system. Besides, it should be highlighted that the jump positions are altered by temperature variations.

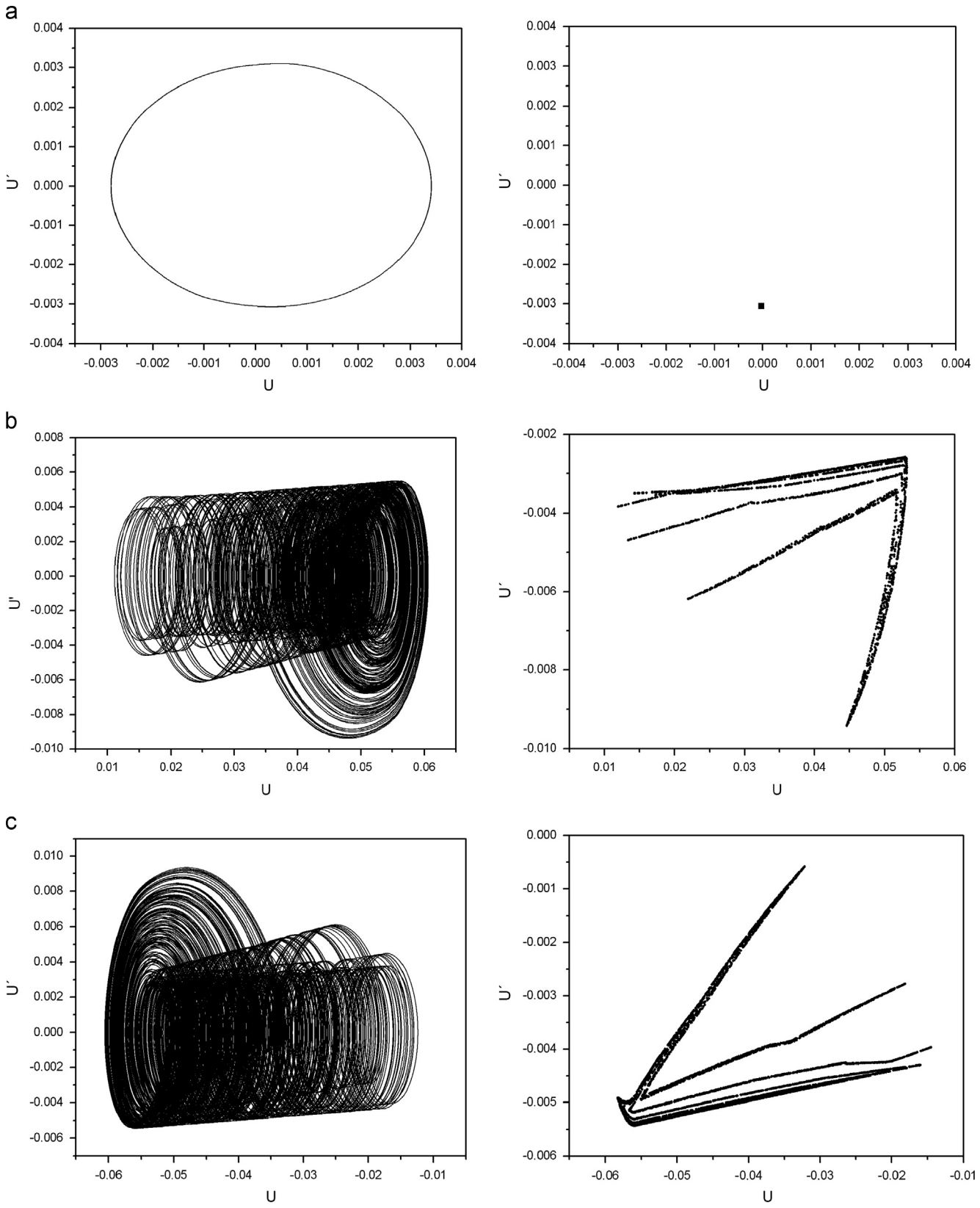

Fig. 11. SMA oscillator multi-stability [54]: (a) Period-1 response; (b) positive chaotic-like response; and (c) negative chaotic-like response.

5. SMA impact system

The use of SMAs in impact systems is now in focus by considering a single-degree of freedom system with an SMA discontinuous support, shown in Fig. 16. The oscillator is composed by a mass m connected by two linear springs with stiffness k. The dissipation process may be modeled by a linear damping with coefficient c. Moreover, the support is massless, having a linear damping with coefficient c_s and also an element that could be either linear elastic or made by SMA. The mass displacement is denoted by x, relative to

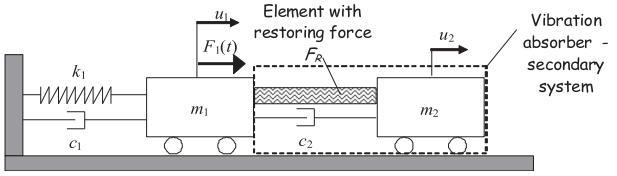

Fig. 12. Vibration absorber connected to a primary system [56].

the equilibrium position, and the distance between the mass and the support is defined by a gap g. Therefore, the system has two possible dynamical modes: with and without contact. Santos and Savi [48] and Sitnikova et al. [62] treated the dynamical behavior of this system. Sitnikova et al. [61] presented an experimental investigation of an impact system with SMA. This system is representative of the dynamical behavior of different applications. For instance, it may be understood as a one-dimensional version of

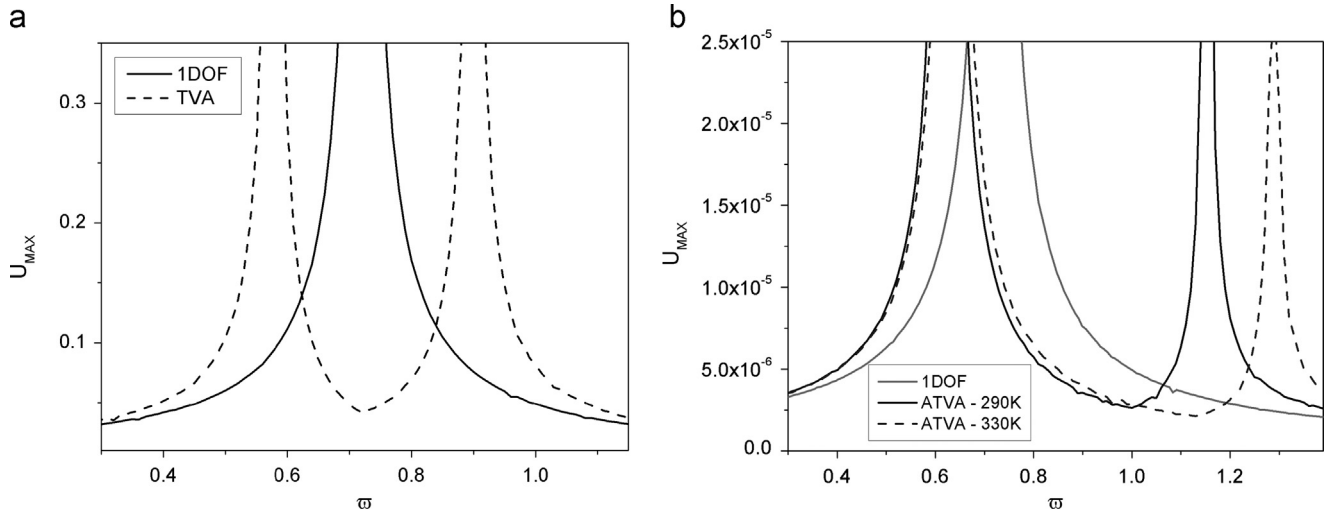

Fig. 13. Maximum amplitudes response of the 1DoF linear oscillator and of the TVA primary system with $\delta=0.01$ [56]. (a) TVA response and (b) SMA–ATVA response for different temperatures.

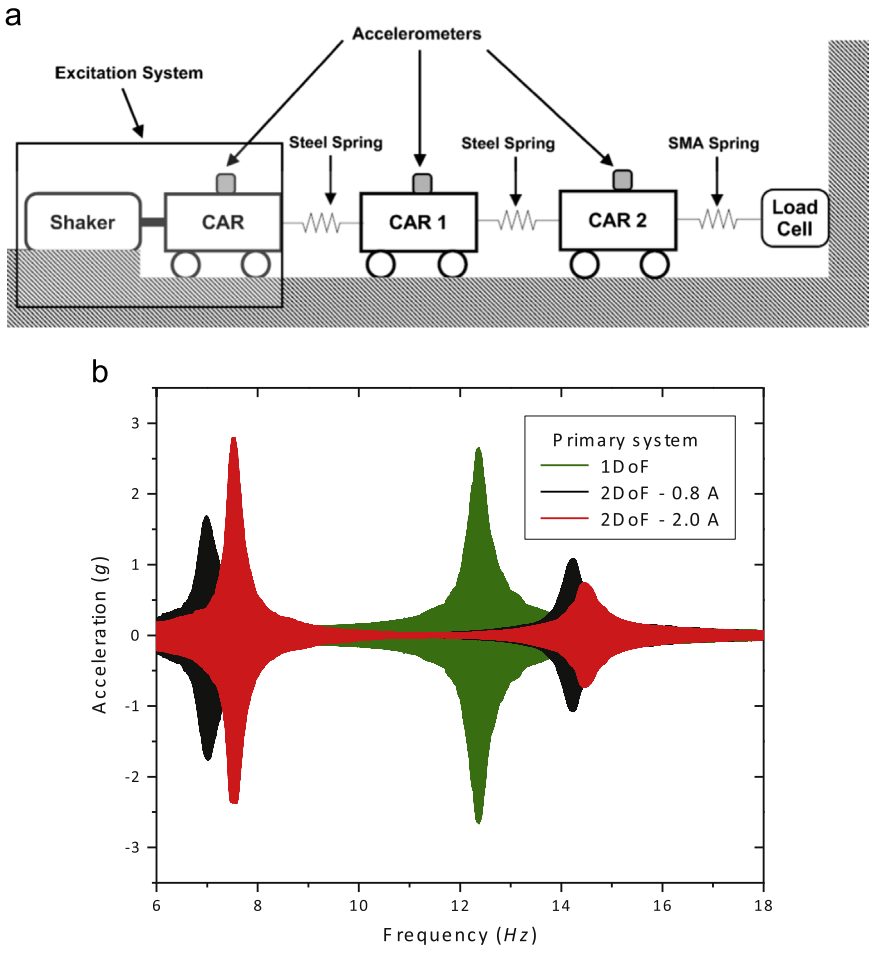

Fig. 14. Experimental SMA oscillator free vibration due to temperature variations Aguiar et al. [3]. (a) Experimental apparatus and (b) sine-sweep tests.

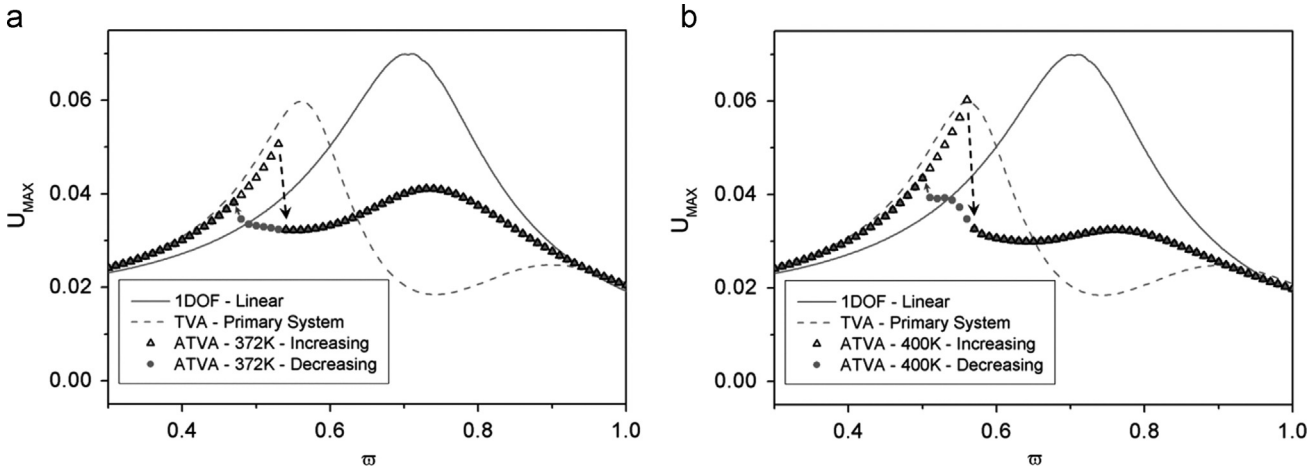

Fig. 15. SMA–ATVA primary system maximum amplitudes response for sine-sweep tests for $\delta=0.01$, $\xi_1=\xi_2=0.2$, and different temperatures [56].

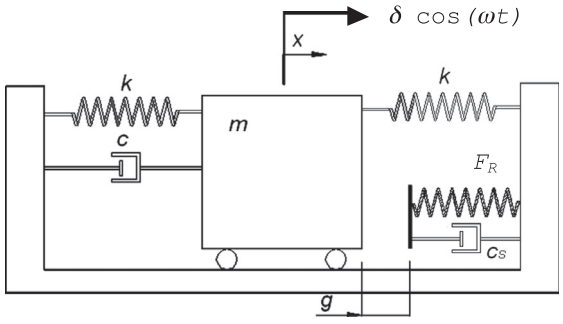

Fig. 16. The SMA impact system [48].

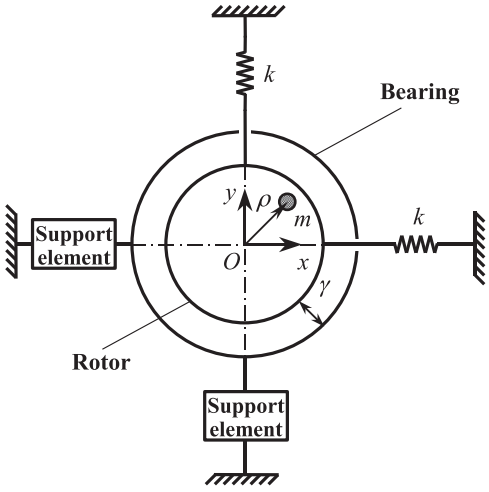

Fig. 17. The rotordynamic nonsmooth system [60].

the rotordynamics problem discussed in Silva et al. [60] and shown in Fig. 17. An analogous system with elastic support was discussed in Savi et al. [55] and the elastic rotordynamic system was discussed in Karpenko et al. [28].

The equations of motion of the impact system can be written as follows [48]:

$$\begin{cases} m\ddot{x}+2kx+c\dot{x}=\delta cos(\omega t), & \text{without contact.} \\ m\ddot{x}+2kx+F_R+(c+c_s)\dot{x}=\delta cos(\omega t), & \text{with contact.} \end{cases} \tag{22}$$

where $F_R=F_R(x-g)$ represents the restitution force of the support element. By assuming an SMA support, its thermomechanical behavior needs to be described by a proper constitutive equation. Here, the one previously presented is employed. On the other hand, the restitution force may be provided by a linear elastic element described by $F_R=k_s(x-g)$.

The nonlinear dynamics analysis of the oscillator with discontinuous support is performed by establishing a comparison with the system with a linear elastic support, highlighting the major differences between them. In order to obtain a global understanding of the system behavior, bifurcation diagrams are presented showing the stroboscopic sample of state variables (displacement and velocity) under the slow quasi-static variation of dissipation parameter c. This analysis shows the influence of dissipation on system dynamics. Linear elastic and SMA support system responses are plotted together in Fig. 18. The elastic support system presents a complex behavior, presenting chaotic-like response for low values of dissipation parameter. The more this parameter is increased, the less complex is the system response. On the other hand, the response of the system with SMA support dissipates energy enough to obtain a less complex behavior for all dissipation parameters.

A specific response is now in focus. Fig. 19 shows the system response for $c=0.05$ Nm/s, a value inside the cloud of points of the bifurcation diagram. The elastic support system response is chaotic-like, presenting a strange attractor with fractal-like structure. On the other hand, the SMA support system presents a periodic response. This difference may be explained by the high dissipation capacity of the SMA system due to hysteresis loop. It should be pointed out that the SMA support introduces dissipation to the system that dramatically changes its response when compared to those obtained from the linear elastic support. Notice that the increase of the system dissipation by changing the dissipation parameter tends to homogenize the behaviors related to both systems.

6. SMA structure

Adaptive structures with SMA actuators may be imagined in several situations related to self-erectable systems, aerospace systems, among others. An archetypal system associated with this kind of structure is the two-bar truss. This kind of systems allows one to analyze bifurcation scenarios related to stability changes associated with different characteristics of buckling behavior. Symmetric two-bar truss, known as the von Mises truss,

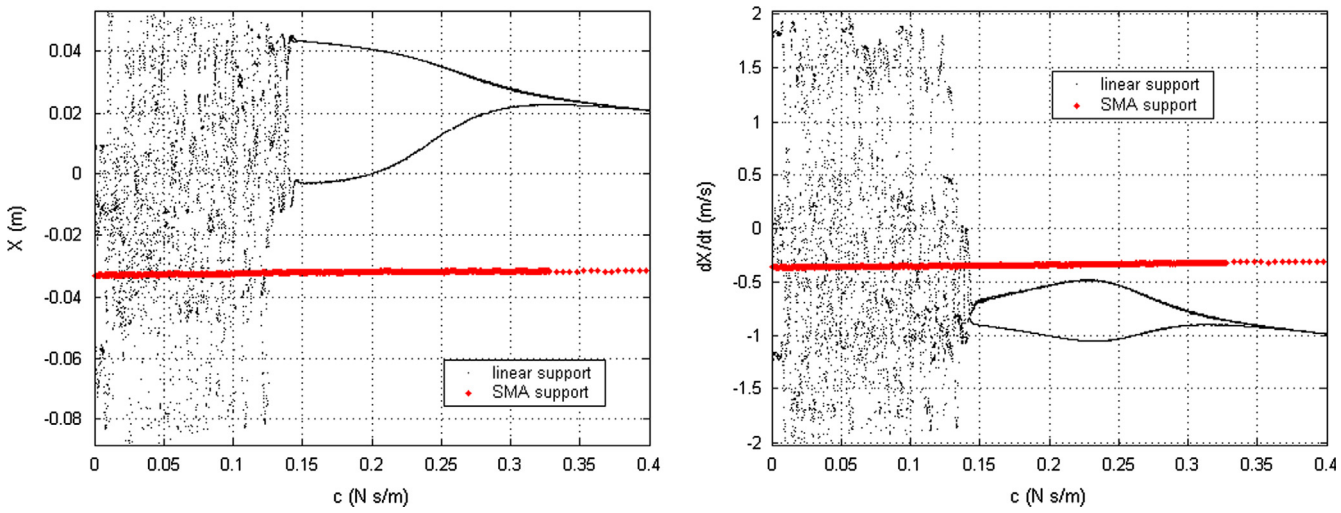

Fig. 18. SMA impact system bifurcation diagrams varying dissipation parameter [48].

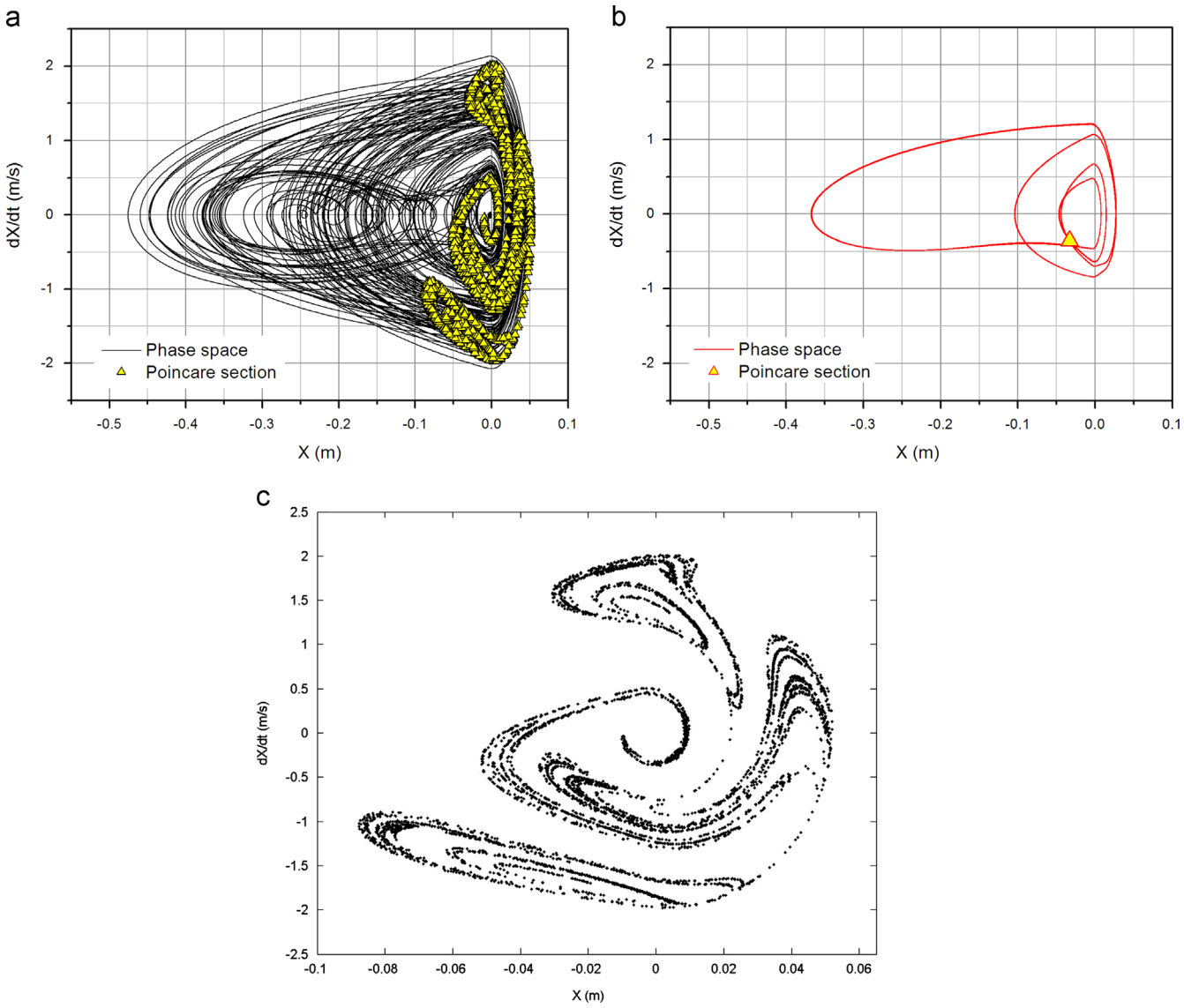

Fig. 19. SMA impact system response for $c=0.05$ Nm/s compared with the elastic impact system [48].

represents one of the most popular system related to stability analysis, defining some of the most important characteristics of framed structures as well as of flat arches and of many other physical phenomena associated with bifurcation buckling.

Savi and Nogueira [57] and Savi et al. [51] discussed the main aspects of the dynamical behavior of SMA two-bar truss by considering two different constitutive models to describe the thermomechanical behavior of SMAs. As depicted in Fig. 20, the two-bar truss is a plane, framed structure, formed by two identical bars, both making an angle φ with a horizontal line, and free to rotate around their supports and at the joint. The structure's mass is lumped at the node, and only vertical, symmetrical motions of the truss are considered. Under these assumptions, the structure is divided into segments without mass, connected by nodes with lumped mass, m. The two identical bars are built with shape memory alloys having length l and cross section area A. The critical Euler load of each bar is assumed to be sufficiently large so that buckling does not occur.

The non-dimensional equation of motion of this structural system is given by the following equations together with constitutive model previously discussed to define volume fractions evolutions [57]:

$$x' = y$$

$$y' = \delta sin(\varpi\tau) - \xi y - \mu_E\left[1 - \frac{1}{(x^2+b^2)^{1/2}}\right]x - [(\hat{\alpha}+\mu_E\alpha_h)(\beta^- - \beta^+) - \hat{\Omega}\mu_\Omega(\theta-\theta_0)]\frac{x}{(x^2+b^2)^{1/2}} \quad (23)$$

The elastic von Mises truss has three equilibrium points due to geometrical nonlinearity. Of those, two are stable while the other one is unstable [8]. In the case of an SMA two-bar truss, constitutive nonlinearity introduces a different behavior. Savi et al. [51] showed how constitutive nonlinearity represented by the polynomial model changes the structure of equilibrium points. The use of the constitutive model with internal constraints previously discussed is more accurate and introduces more differences to the original structure of the two-bar truss related to the geometrical nonlinearity.

Results from free vibration simulations are presented in the form of phase portraits. Fig. 21 presents the free-response of the SMA system. For high temperature (θ=1.28), where there is only austenitic phase for a stress-free state, the system has one unstable and two stable equilibrium points (Fig. 21a). This situation is similar to the geometrical nonlinear system in terms of number of equilibrium points, however, it should be highlighted that the SMA system tends to dissipate energy due to the hysteresis loop. On the other hand, at low temperatures (θ=0.99), where martensitic phase is stable in a stress-free state, the system has 11 equilibrium points where six are stable and five are unstable (Fig. 21b). Note that constitutive nonlinearity induces the formation of five equilibrium points at the upper position of the truss, and other five at the lower position. From each of those sets, three are stable while the others are unstable. These characteristics are related to the stability of martensitic variants.

Forced vibration analysis is now in focus by considering high temperature behavior that is related to the pseudoelastic effect where austenitic phase is stable in stress-free state. Initially, the bifurcation diagram is of concern showing stroboscopically

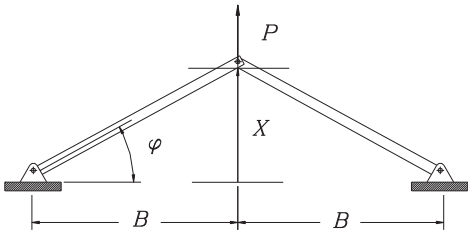

Fig. 20. SMA two-bar truss [57,51].

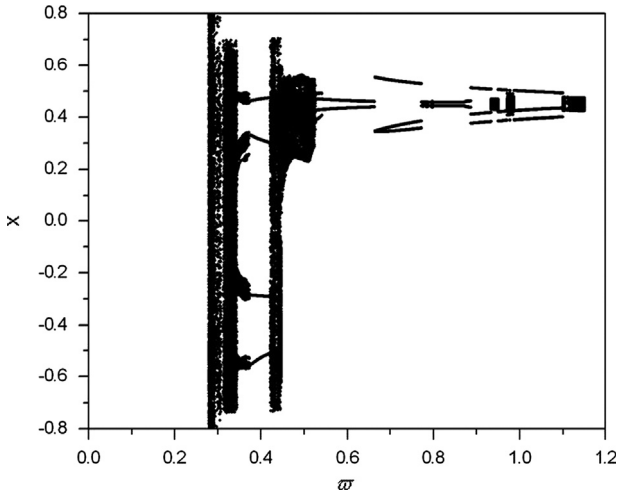

Fig. 22. SMA two-bar truss bifurcation diagram varying ϖ with δ=0.01 [57].

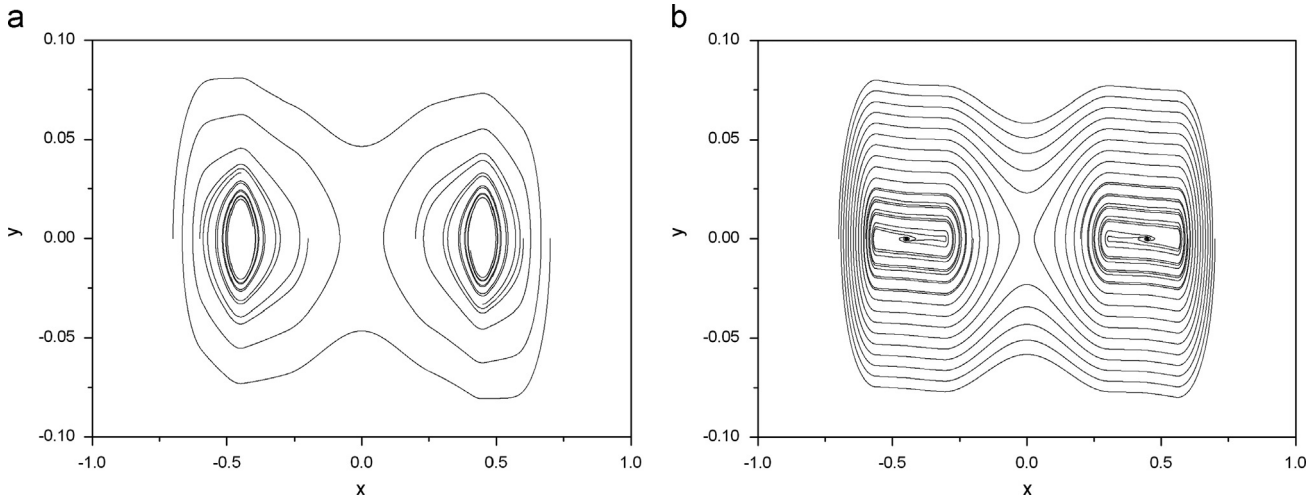

Fig. 21. Free vibration of the SMA two-bar truss [57].

sampled displacement values under the slow quasi-static increase of a system parameter. The driving frequency, ϖ, is of concern, assuming a fixed forcing amplitude $\delta=0.01$. Fig. 22 presents this bifurcation diagram showing regions related to cloud of points and also regions represented by a discrete number of points associated with periodic motions.

Different frequency values are now investigated in order to analyze the system response. Phase space plots and Poincaré sections are presented for each set of parameters. For this forcing amplitude value, when frequency is $\varpi=0.382$, a period-2 motion occurs, oscillating around the truss lower position equilibrium point (Fig. 23a). The Poincaré section presents two points. When $\varpi=0.42$, the system stills presenting a period-2 motion, however, at a different position. Now, the system oscillates around the truss upper position (Fig. 23b). A quasi-periodic motion also appears for $\varpi=0.9418$, presenting a closed curve at the Poincaré section [57]. All these possibilities represent the great complexity related to the SMA two-bar truss dynamical behavior.

Chaotic motion is also a possibility related to the pseudoelastic two-bar truss. By considering $\varpi=0.3347$, it is noticeable a chaotic-like motion related to a typical strange attractor observed in the Poincaré section (Fig. 24a). Note that this motion is related to all phase space, visiting all equilibrium points. A different chaotic motion may be induced when $\varpi=0.475$. Under this condition, the system tends to oscillate only at the truss upper position and the strange attractor is restricted to the positive part of the phase plane (Fig. 24b). Since there is attractor coexistence, the position of the chaotic attractor may be altered by considering proper initial conditions. Fig. 24c presents the chaotic strange attractor visiting the truss lower position.

Chaos control is an alternative to stabilize unstable periodic orbits embedded in chaotic attractor, providing a way to track desirable orbits with small power consumption. This approach can be useful to confer flexibility to the system that can quickly react to new situations. Besides, it can avoid undesirable situations related to distinct bifurcation scenarios. De Paula and Savi [18] provided a general overview of chaos control techniques, establishing a comparative analysis among them. De Paula et al. [20] discussed their use to bifurcation control, which is useful for structural systems. Bessa et al. [13] and De Paula et al. [21] presented this strategy in the SMA two-bar truss.

7. Conclusions

This paper deals with nonlinear dynamics and chaos in the shape memory alloy system, presenting a collection of results related to different dynamical systems. Basically, single degree of freedom oscillators, vibration absorbers, impact systems and two-bar trusses are treated. In general, dynamical response is very rich,

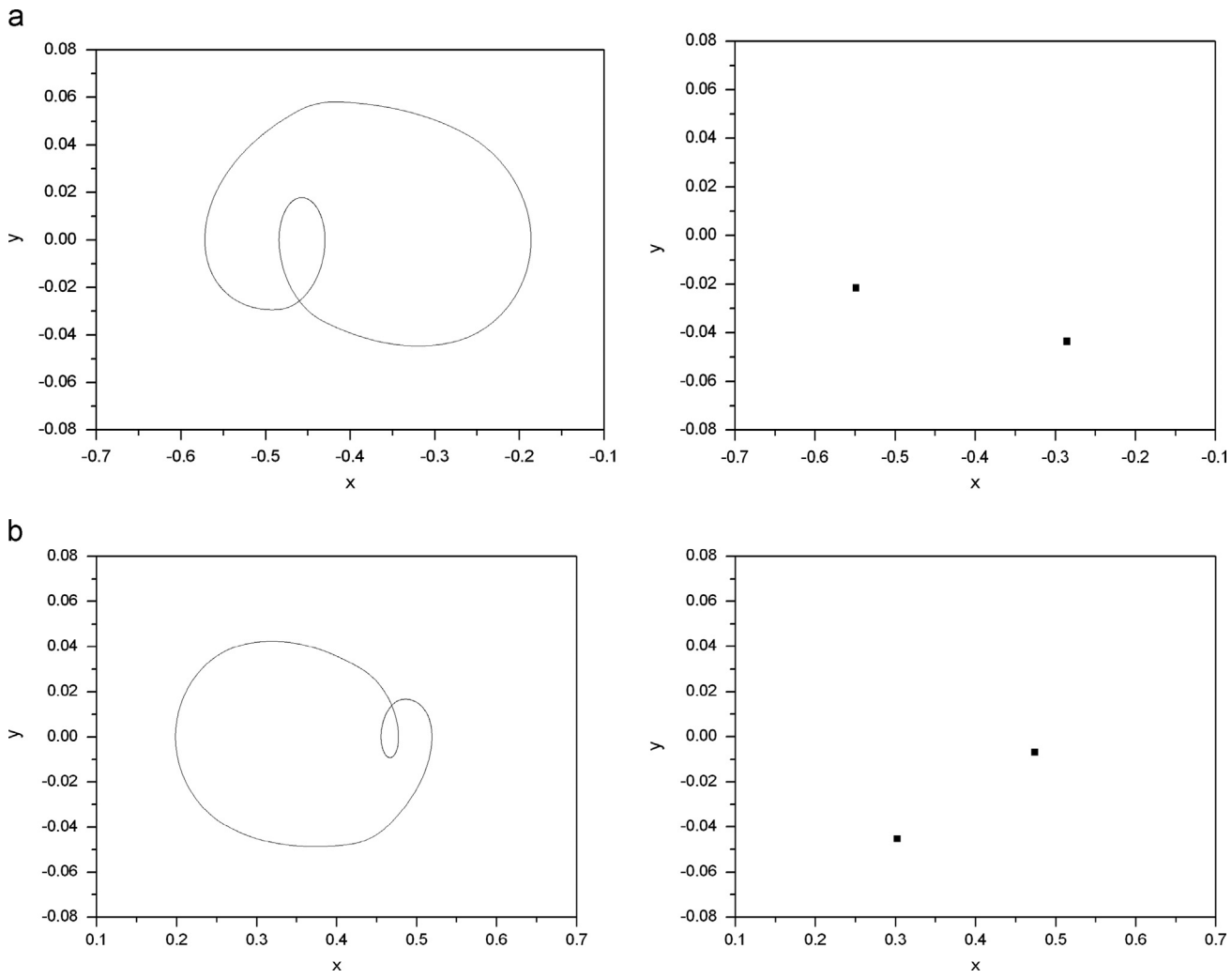

Fig. 23. SMA two-bar truss [57]: (a) period-2 response for $\delta=0.01$ and $\varpi=0.382$, oscillating around the truss lower position; (b) period-2 response for $\delta=0.01$ and $\varpi=0.42$, oscillating around the truss upper position.

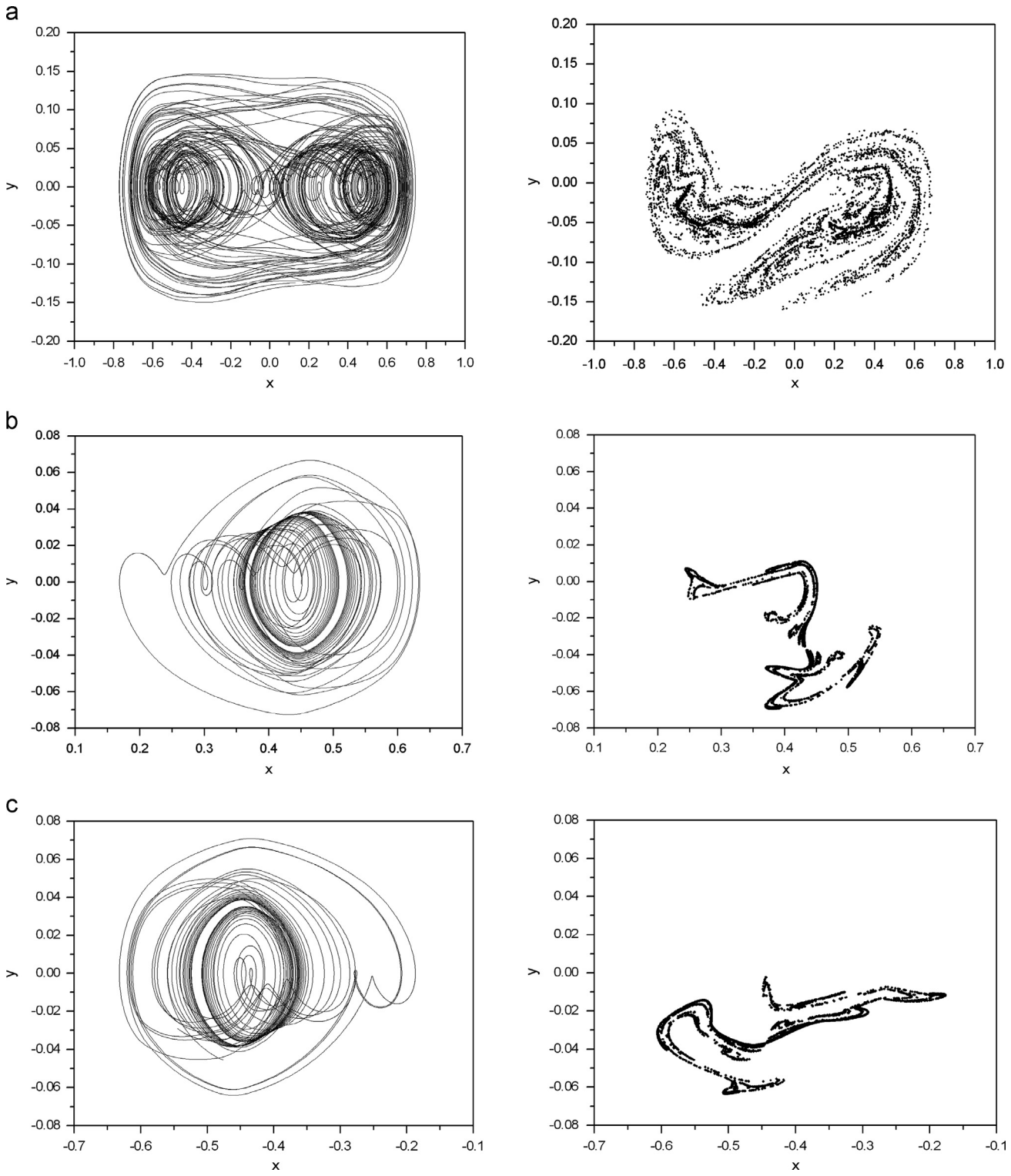

Fig. 24. SMA two-bar truss chaotic like responses [57]: (a) $\delta=0.01$ and $\varpi=0.3347$ visiting the whole space; (b) $\delta=0.01$ and $\varpi=0.475$ visiting the truss upper position; and (c) $\delta=0.01$ and $\varpi=0.475$ visiting the truss lower position.

including periodic, quasi-periodic and chaotic behaviors. Multistability is also present characterizing attractors coexistence. Dynamical jumps are another important aspect of SMA system response. In general, the SMA system presents several equilibrium points, and the number and characteristics are defined by temperature. Therefore, it is possible to imagine position actuation with SMA elements. Property alterations due to phase transformation are another remarkable characteristic of the SMA dynamical system. Essentially, it can be exploited changing resonant conditions. The hysteretic behavior may be also exploited generating a smart dissipation that actuates only for high amplitudes. It should be pointed out that there is a competition between property changes and hysteretic behavior, defining the system response. All these aspects can be exploited to generate smart adaptive systems. Vibration absorbers, for instance, is capable of reducing the system response amplitudes not only on the initially chosen

forcing frequency but in distinct situations considering temperature variations. Nevertheless, SMAs may introduce unusual, complex dynamical responses that should be investigated during the design of the application. Experimental results confirm the general aspects discussed in this paper.

Acknowledgments

This review paper presents a collection of results developed during the years by my research team. Everything is the fruit of a lot of effort of several colleagues that I need to acknowledge and express my gratitude. Specially, it is important to mention: Pedro M.C.L. Pacheco (CEFET/RJ); Aline S. de Paula (UnB); Dimitris C. Lagoudas (Texas A&M University); Arthur M.B. Braga (PUC-Rio); Alberto Paiva (UFF); Ricardo A.A. Aguiar (CEFET/RJ); Sergio A. Oliveira (COPPE/UFRJ); Paulo C.C. Monteiro Jr. (COPPE/UFRJ); Bruno C. dos Santos (Petrobras); Milton A.N. Sa (Petrobras); Jefferson B. Nogueira (Petrobras).

The author would also like to acknowledge the support of the Brazilian Research Agencies CNPq, CAPES and FAPERJ and through the INCT-EIE (National Institute of Science and Technology – Smart Structures in Engineering) the CNPq and FAPEMIG. The Air Force Office of Scientific Research (AFOSR) is also acknowledged.

References

[1] M.A. Acar, C. Yilmaz, Design of an adaptive–passive dynamic vibration absorber composed of a string–mass system equipped with negative stiffness tension adjusting mechanism, J. Sound Vib. 332 (2) (2013) 231–245.
[2] R.A.A. Aguiar, M.A. Savi, P.M.C.L. Pacheco, Experimental and numerical investigations of shape memory alloy helical springs, Smart Mater. Struct. 19 (2) (2010) 1–9 (Article 025008).
[3] R.A.A. Aguiar, M.A. Savi, P.M.C.L. Pacheco, Experimental investigation of vibration reduction using shape memory alloys, J. Intell. Mater. Syst. Struct. 24 (2) (2013) 247–261.
[4] F.P. Amarante dos Santos, C. Cismaşiu, J. Pamies Teixeira, Semi-active vibration control device based on superelastic NiTi wires, Struct. Control Health Monit. 20 (2013) 890–902.
[5] F. Auricchio, E. Sacco, A temperature-dependent beam for shape-memory alloys: constitutive modeling, finite-element implementation and numerical simulations, Comput. Methods Appl. Mech. Eng. 174 (1–2) (1999) 171–190.
[6] F. Auricchio, D. Fugazza, R. DesRoches, Numerical and experimental evaluation of the damping properties of shape-memory alloys, J. Eng. Mater. Technol. – ASME, 128, 2006312–319.
[7] A.P. Baêta-Neves, M.A. Savi, P.M.C.L. Pacheco, On the Fremond's constitutive model for shape memory alloys, Mech. Res. Commun. 31 (6) (2004) 677–688.
[8] Z.P. Bazant, L. Cedolin, Stability of Structures, World Scientific Publishing Co., NJ, 2010.
[9] D. Bernardini, G. Rega, Thermomechanical modelling, nonlinear dynamics and chaos in shape memory oscillators, Math. Comput. Model. Dyn. Syst. 11 (3) (2005) 291–314.
[10] D. Bernardini, G. Rega, The influence of model parameters and of the thermomechanical coupling on the behavior of shape memory devices, Int. J. Non-linear Mech. 45 (10) (2010) 933–946.
[11] D. Bernardini, G. Rega, Chaos robustness and strength in thermomechanical shape memory oscillators. Part I: a predictive theoretical framework for the pseudoelastic behavior, Int. J. Bifurc. Chaos 21 (10) (2011) 2769–2782.
[12] D. Bernardini, G. Rega, Chaos robustness and strength in thermomechanical shape memory oscillators. Part II: numerical and theoretical evaluation, Int. J. Bifurc. Chaos 21 (10) (2011) 2783–2800.
[13] W.M. Bessa, A.S. de Paula, M.A. Savi, Adaptive fuzzy sliding mode control of smart structures, Eur. Phys. J. – Spec. Top. 222 (7) (2013) 1541–1551.
[14] M.J. Brennan, Some recent developments in adaptive tuned vibration absorbers/neutralisers, Shock Vib. 13 (4–5) (2006) 531–543.
[15] E. Choi, S.-H. Park, Y.-S. Chung, H.S. Kim, Seismic fragility analysis of lap-spliced reinforced concrete columns retrofitted by SMA wire jackets, Smart Mater. Struct. 22 (2013) 1–11 (Article 085028).
[16] M. Collet, E. Foltête, C. Lexcellent, Analysis of the behavior of a shape memory alloy beam under dynamical loading, Eur. J. Mech. A – Solids 20 (4) (2001) 615–630.
[17] A. Czechowicz, On the functional characteristics of pseudoelastic adaptive resetting of shape memory actuators in the field of automotive applications, J. Intell. Mater. Syst. Struct. 24 (13) (2013) 1539–1545.
[18] A.S. De Paula, M.A. Savi, Comparative analysis of chaos control methods: a mechanical system case study, Int. J. Non-linear Mech. 46 (8) (2011) 1076–1089.
[19] A.S. De Paula, M.A. Savi, D.C. Lagoudas, Nonlinear dynamics of a SMA large-scale space structure, J. Braz. Soc. Mech. Sci. Eng. 34 (2012) 401–412.
[20] A.S. De Paula, M.A. Savi, M. Wiercigroch, E. Pavlovskaia, Bifurcation control of a parametric pendulum, Int. J. Bifurc. Chaos 22 (5) (2012) 1–14 (Article 1250111).
[21] A.S. De Paula, M.V.S. dos Santos, M.A. Savi, W.M. Bessa. Controlling a shape memory alloy two-bar truss using delayed feedback method, Int. J. Struct. Stab. Dyn., (submitted for publication).
[22] L. Dieng, G. Helbert, S.A. Chirani, T. Lecompte, P. Pilvin, Use of shape memory alloys damper device to mitigate vibration amplitudes of bridge cables, Eng. Struct. 56 (2013) 1547–1556.
[23] O. Doaré, A. Sbarra, C. Touzé, M.O. Moussa, Z. Moumni, Experimental analysis of the quasi-static and dynamic torsional behaviour of shape memory alloys, Int. J. Solids Struct. 49 (1) (2012) 32–42.
[24] M. Fremond, Shape memory alloy: a thermomechanical macroscopic theory, CISM Courses and Lectures, vol. 351, 1996.
[25] A.A. Gholampour, M. Ghassemieh, J. Kiani, State of the art in nonlinear dynamic analysis of smart structures with SMA members, Int. J. Eng. Sci. 75 (2014) 108–117.
[26] M. Hajianmaleki, M.S. Qatu, Vibrations of straight and curved composite beams: a review, Compos. Struct. 100 (2013) 218–232.
[27] R.A. Ibrahim, Recent advances in nonlinear passive vibration isolators, J. Sound Vib. 314 (3–5) (2008) 371–452.
[28] E.V. Karpenko, M. Wiercigroch, M.P. Cartmell, Regular and chaotic dynamics of a discontinuously nonlinear rotor system, Chaos Solitons Fractals 13 (6) (2002) 1231–1242.
[29] S.M.R. Khalili, M. Botshekanan Dehkordi, E. Carrera, M. Shariyata, Non-linear dynamic analysis of a sandwich beam with pseudoelastic SMA hybrid composite faces based on higher order finite element theory, Compos. Struct. 96 (2013) 243–255.
[30] W. Lacarbonara, F. Vestroni, Nonclassical responses of oscillators with hysteresis, Nonlinear Dyn. 32 (2003) 235–258.
[31] W. Lacarbonara, D. Bernardini, F. Vestroni, Nonlinear thermomechanical oscillations of shape-memory devices, Int. J. Solids Struct. 41 (5–6) (2004) 1209–1234.
[32] D.C. Lagoudas, Shape Memory Alloys: Modeling and Engineering Applications, Springer, New York, 2008.
[33] J. Lemaitre, J.L. Chaboche, Mechanics of Solid Materials, Cambridge University Press, New York, 1990.
[34] G. Litak, D. Bernardini, A. Syta, G. Rega, A. Rysak, Analysis of chaotic non-isothermal solutions of thermomechanical shape memory oscillators, Eur. Phys. J. – Spec. Top. 222 (7) (2013) 1637–1647.
[35] L.G. Machado, M.A. Savi, Medical applications of shape memory alloys, Braz. J. Med. Biol. Res. 36 (6) (2003) 683–691.
[36] L.G. Machado, M.A. Savi, P.M.C.L. Pacheco, Nonlinear dynamics and chaos in coupled shape memory oscillators, Int. J. Solids Struct. 40 (19) (2003) 5139–5156.
[37] L.G. Machado, M.A. Savi, P.M.C.L. Pacheco, Bifurcations and crises in a shape memory oscillator, Shock Vib. 11 (2) (2004) 67–80.
[38] L.G. Machado, D.C. Lagoudas, M.A. Savi, Lyapunov exponents estimation for hysteretic systems, Int. J. Solids Struct. 46 (6) (2009) 1269–1598.
[39] P.C.C. Monteiro Jr., M.A. Savi, T.A. Netto, P.M.C.L. Pacheco, A phenomenological description of the thermomechanical coupling and the rate-dependent behavior of shape memory alloys, J. Intell. Mater. Syst. Struct. 20 (14) (2009) 1675–1687.
[40] P.C.C. Monteiro Jr., L.L. Silva, T.A. Netto, M.A. Savi, Experimental investigation of the influence of the heating rate in an SMA actuator performance, Sens. Actuat. A – Phys. 199 (2013) 254–259.
[41] S.A. Oliveira, M.A. Savi, A.L. Kalamkarov, A three-dimensional constitutive model for shape memory alloys, Arch. Appl. Mech. 80 (10) (2010) 1163–1175.
[42] H.S. Oliveira, A.S. De Paula, M.A. Savi, Dynamical jumps in a shape memory alloys oscillator, Shock Vib., (in press).
[43] M. Ortiz, P.M. Pinsky, R.L. Taylor, Operator split methods for the numerical solution of the elastoplastic dynamic problem, Comput. Methods Appl. Mech. Eng. 39 (1983) 137–157.
[44] A. Paiva, M.A. Savi, A.M.B. Braga, P.M.C.L. Pacheco, A constitutive model for shape memory alloys considering tensile-compressive asymmetry and plasticity, Int. J. Solids Struct. 42 (11–12) (2005) 3439–3457.
[45] A. Paiva, M.A. Savi, An overview of constitutive models for shape memory alloys, Math. Probl. Eng. 2006 (2006) 1–30 (Article ID56876).
[46] P. Popov, D.C. Lagoudas, A 3-D constitutive model for shape memory alloys incorporating pseudoelasticity and detwinning of self-accommodated martensite, Int. J. Plast. 23 (2007) 1679–1720.
[47] S. Saadat, J. Salichs, M. Noori, Z. Hou, H. Davoodi, I. Bar-On, Y. Suzuki, A. Masuda, An overview of vibration and seismic applications of NiTi shape memory alloy, Smart Mater. Struct. 11 (2) (2002) 218–229.
[48] B.C. Santos, M.A. Savi, Nonlinear dynamics of a nonsmooth shape memory alloy oscillator, Chaos Solitons Fractals 40 (1) (2007) 197–209.
[49] M.A. Savi, A.M.B. Braga, Chaotic vibrations of an oscillator with shape memory, J. Braz. Soc. Mech. Sci. Eng. 15 (1) (1993) 1–20.
[50] M.A. Savi, P.M.L.C. Pacheco, Chaos and hyperchaos in shape memory systems, Int. J. Bifurc. Chaos 12 (3) (2002) 645–657.
[51] M.A. Savi, P.M.C.L. Pacheco, A.M.B. Braga, Chaos in a shape memory two-bar truss, Int. J. Non-linear Mech. 37 (8) (2002) 1387–1395.
[52] M.A. Savi, A. Paiva, A.P. Baêta-Neves, P.M.C.L. Pacheco, Phenomenological modeling and numerical simulation of shape memory alloys: a thermo-

plastic-phase transformation coupled model, J. Intell. Mater. Syst. Struct. 13 (5) (2002) 261–273.
[53] M.A. Savi, A. Paiva, Describing internal subloops due to incomplete phase transformations in shape memory alloys, Arch. Appl. Mech. 74 (9) (2005) 637–647.
[54] M.A. Savi, M.A.N. Sa, A. Paiva, P.M.C.L. Pacheco, Tensile-compressive asymmetry influence on the shape memory alloy system dynamics, Chaos Solitons Fractals 36 (4) (2006) 828–842.
[55] M.A. Savi, S. Divenyi, L.F.P. Franca, H.I. Weber, Numerical and experimental investigations of the nonlinear dynamics and chaos in non-smooth systems, J. Sound Vib. 30 (1–2) (2007) 59–73.
[56] M.A. Savi, A.S. De Paula, D.C. Lagoudas, Numerical investigation of an adaptive vibration absorber using shape memory alloys, J. Intell. Mater. Syst. Struct. 22 (1) (2011) 67–80.
[57] M.A. Savi, J.B. Nogueira, Nonlinear dynamics and chaos in a pseudoelastic two-bar truss, Smart Mater. Struct. 19 (11) (2010) 1–11 (Article 1150222010).
[58] M. Shariyat, M. Moradi, S. Samaee, Enhanced model for nonlinear dynamic analysis of rectangular composite plates with embedded SMA wires, considering the instantaneous local phase changes, Compos. Struct. 109 (2014) 106–118.
[59] J.A. Shaw, S. Kyriakides, Thermomechanical aspects of Ni–Ti, J. Mech. Phys. Solids 43 (8) (1995) 1243.
[60] L.C. Silva, M.A. Savi, A. Paiva, Nonlinear dynamics of a rotordynamic non-smooth shape memory alloy system, J. Sound Vib. 332 (3–4) (2013) 608–621.
[61] E. Sitnikova, E. Pavlovskaia, J. Ing, M. Wiercigroch, Experimental bifurcations of an impact oscillator with SMA constraint, Int. J. Bifurc. Chaos 22 (5) (2012) 1–19.
[62] E. Sitnikova, E. Pavlovskaia, M. Wiercigroch, M.A. Savi, Vibration reduction of the impact system by an SMA restraint: numerical studies, Int. J. Non-linear Mech. 45 (2010) 837–849.
[63] L. Wang, R.V.N. Melnik, Nonlinear dynamics of shape memory alloy oscillators in tuning structural vibration frequencies, Mechatronics 22 (8) (2012) 1085–1096.
[64] K. Williams, G. Chiu, R. Bernhard, Adaptive–passive absorbers using shape-memory alloys, J. Sound Vib. 249 (5) (2002) 835–848.
[65] K. Williams, G. Chiu, R. Bernhard, Dynamic modelling of a shape memory alloy adaptive tuned vibration absorber, J. Sound Vib. 280 (2005) 211–234.
[66] S.H. Yoon, Experimental investigation of thermo-mechanical behaviors in Ni–Ti shape memory alloy, J. Intell. Mater. Syst. Struct. 19 (3) (2008) 283–289.